Molecular Cell

Article

Exportin-1 functions as an adaptor for transcription factor-mediated docking of chromatin at the nuclear pore complex

Graphical abstract

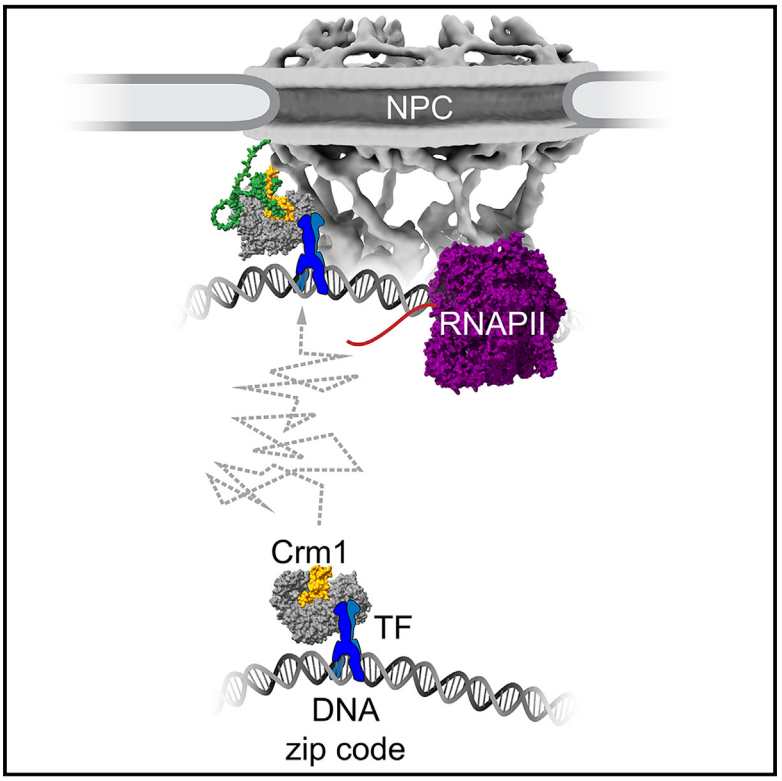

Authors

Tiffany Ge, Donna Garvey Brickner, Kara Zehr, ..., Brian Chait, Michael P. Rout, Jason H. Brickner

Correspondence

j-brickner@northwestern.edu

In brief

Many genes physically interact with the nuclear pore complex (NPC), which requires transcription factors (TFs). Ge et al. show that the exportin Crm1 binds TFs and nuclear pore proteins to dock chromatin at the NPC and to stimulate transcription. This function of Crm1 is distinct from its role in nuclear export.

Highlights

- Crm1 co-occupies hundreds of enhancers and promoters with nuclear pore proteins
- Crm1 functions upstream of Nups to mediate peripheral targeting of genes
- Crm1 and Nup2 promote nascent transcription of hundreds of genes
- Crm1 binding to the Gcn4 TF and Nup2 is mechanistically distinct from NES binding

Ge et al., 2025, Molecular Cell *85*, 1101–1116
March 20, 2025
https://doi.org/10.1016/j.molcel.2025.02.013

CellPress

Molecular Cell

CellPress

Article

Exportin-1 functions as an adaptor for transcription factor-mediated docking of chromatin at the nuclear pore complex

Tiffany Ge,[1] Donna Garvey Brickner,[1] Kara Zehr,[1] D. Jake VanBelzen,[1] Wenzhu Zhang,[2] Christopher Caffalette,[3] Gavin C. Moeller,[4] Sara Ungerleider,[1] Nikita Marcou,[1,5] Alexis Jacob,[1] Vu Q. Nguyen,[4] Brian Chait,[2] Michael P. Rout,[3] and Jason H. Brickner[1,6,*]

[1]Department of Molecular Biosciences, Northwestern University, Evanston, IL 60201, USA
[2]Laboratory of Mass Spectrometry and Gaseous Ion Chemistry, The Rockefeller University, New York, NY 10065, USA
[3]Laboratory of Cellular and Structural Biology, The Rockefeller University, New York, NY, USA
[4]Department of Molecular Biology, School of Biological Sciences, University of California, San Diego, La Jolla, San Diego, CA 92093, USA
[5]Present address: Department of Genetic Medicine, Johns Hopkins School of Medicine, Baltimore, MD 21205, USA
[6]Lead contact
*Correspondence: j-brickner@northwestern.edu
https://doi.org/10.1016/j.molcel.2025.02.013

SUMMARY

Nuclear pore proteins (nucleoporins [Nups]) physically interact with hundreds of chromosomal sites, impacting transcription. In yeast, transcription factors mediate interactions between Nups and enhancers and promoters. To define the molecular basis of this mechanism, we exploited a separation-of-function mutation in the Gcn4 transcription factor that blocks its interaction with the nuclear pore complex (NPC). This mutation reduces the interaction of Gcn4 with the highly conserved nuclear export factor Crm1/Xpo1. Crm1 and Nups co-occupy enhancers, and Crm1 inhibition blocks interaction of the nuclear pore protein Nup2 with the genome. *In vivo*, Crm1 interacts stably with the NPC and *in vitro*, Crm1 binds directly to both Gcn4 and Nup2. Importantly, the interaction between Crm1 and Gcn4 requires neither Ran-guanosine triphosphate (GTP) nor the nuclear export sequence binding site. Finally, Crm1 and Ran-GTP stimulate DNA binding by Gcn4, suggesting that allosteric coupling between Crm1-Ran-GTP binding and DNA binding facilitates the docking of transcription-factor-bound enhancers at the NPC.

INTRODUCTION

Nuclear pore complexes (NPCs) are large proteinaceous channels spanning the nuclear envelope that mediate trafficking of macromolecules between the cytoplasm and the nucleus. These 8-fold symmetrical ring structures are composed of 16–48 copies of ~30 different pore proteins called nucleoporins (Nups).[1–3] In addition to their transport function, Nups also physically associate with the genomes of budding yeast, flies, and mammals.[4–9] Whereas interaction with Nups correlates with localization of chromatin at the nuclear periphery in yeast, such chromatin-Nup interactions occur both at the periphery and in the nucleoplasm in flies and mammals.[8,10] Furthermore, the nuclear envelope can invaginate into the nucleoplasm to contact chromatin.[11] Although chromatin-Nup interactions are associated with stronger transcription, DNA repair, chromosome folding, gene silencing, and epigenetic transcriptional poising,[4,12–20] the molecular mechanism(s) by which Nups are recruited to chromatin is not well understood.

An excellent model for Nup-genome interactions is the recruitment of inducible genes to the NPC in budding yeast.[7,12] Many active genes interact with Nups,[7] and inducible genes often reposition to the NPC upon activation. Repositioning requires several Nups, including the nucleoplasmic proteins Nup1, Nup2, and Nup60.[13,14,20,21] Although peripheral localization does not require active transcription,[13,22] it does require transcription factors (TFs) and their binding sites.[14,20,23,24] These TF binding sites function as *DNA zip codes* that are sufficient to induce peripheral localization at an ectopic locus.[14,20,23] Loss of TFs or zip codes disrupts peripheral localization and leads to a quantitative decrease in transcription.[14,25] Nups also promote transcription in flies, plants, and mammals.[9,10,26,27]

Several yeast TFs mediate peripheral localization: Cbf1, Gcn4, Put3, Sfl1, and Ste12.[23,24,28] This is likely a common function of yeast TFs; when tethered to an ectopic locus, ~65% of yeast DNA binding proteins promote Nup2-dependent repositioning to the nuclear periphery.[29] Likewise, in mammals, Nups interact strongly with super-enhancers that are rich in TF binding sites.[30]

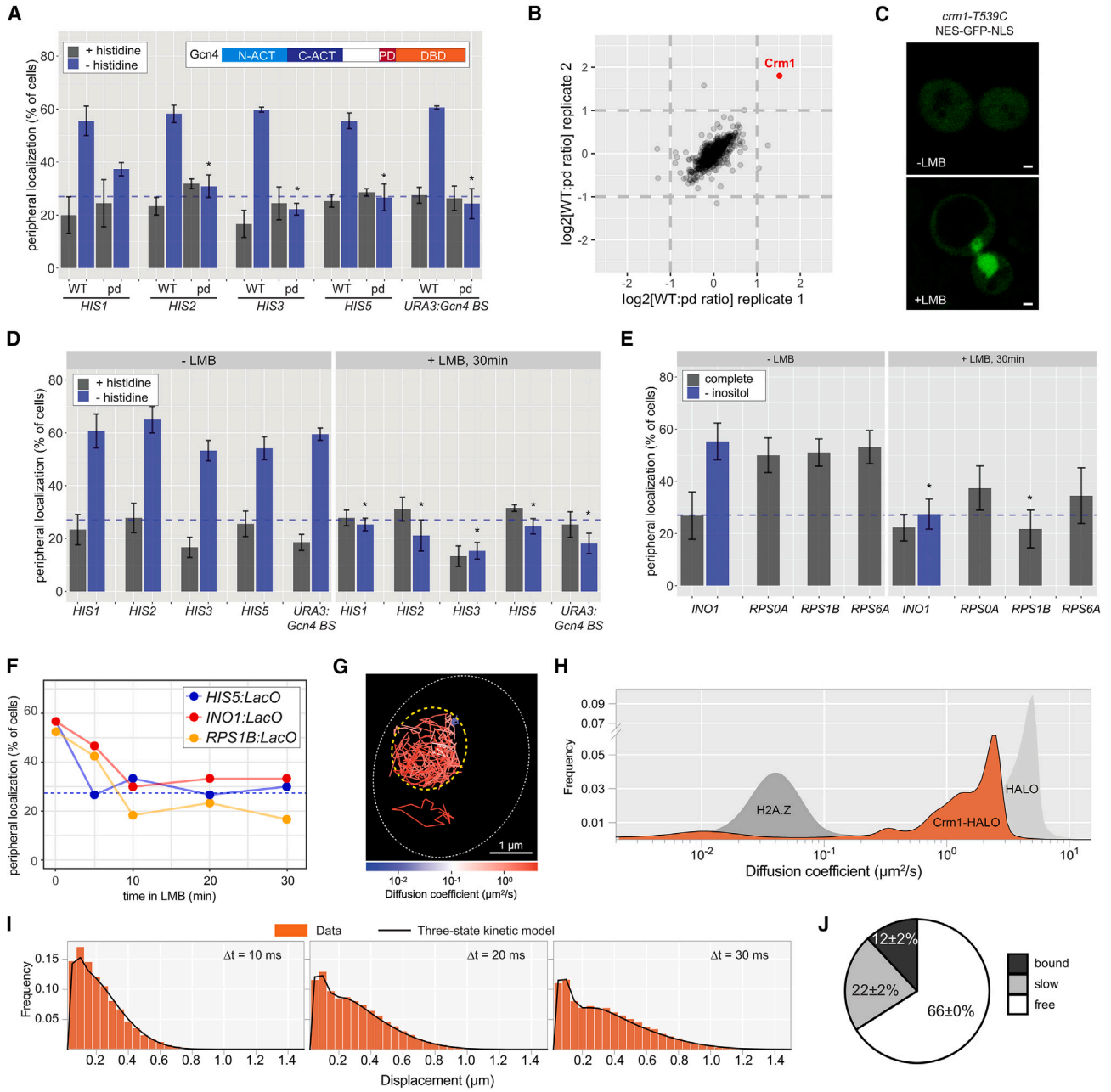

Figure 1. Crm1/Xpo1 is essential for peripheral localization of both Gcn4-dependent and Gcn4-independent genes

(A and D–F) Peripheral localization of the indicated genes or the Gcn4 binding site inserted at an ectopic locus (*URA3:Gcn4BS*). Mean ± SEM from ≥3 biological replicates of ≥30 cells each. Dashed line: localization expected for a randomly positioned gene.[12]

(A) Wild-type or *gcn4-pd*-mutant strains grown in SDC ± histidine. Inset: domain structure of Gcn4.[29]

(B) Scatterplot of the ratio of normalized abundance of 759 proteins identified by stable isotope labeling by amino acids in cell culture (SILAC) mass spectrometry (MS) comparing the recovery from wild-type (JBY558; light) and mutant (JBY557; heavy) cultures starved for histidine for 1 h, with Crm1 highlighted.

(C) LMB-sensitive strain (*crm1-T539C*) expressing GFP bearing both a nuclear localization signal and a nuclear export signal (NES-GFP-NLS) ± 100 ng/mL LMB, 30 min.

(D and E) Gcn4 target genes (D) or non-Gcn4 target genes (E) in *crm1-T539C* grown in the indicated media treated ±100 ng/mL LMB. For (E), strains were grown in complete medium or ± inositol (*INO1:LacO*).

(F) Time courses of peripheral localization of *HIS5*, *RPS1B*, and *INO1* following addition of LMB.

(legend continued on next page)

Structure-function analysis of the yeast TF Gcn4 identified a 27-amino acid fragment (aa 205–231) outside the DNA binding and activation domains, which is sufficient to mediate peripheral localization (Figure 1A).[29,31] Point mutations in PD_{GCN4} disrupt Gcn4-mediated peripheral localization and reduce transcription.[29,32] Thus, controlling interaction with the NPC represents a separate function that is encoded within the aa sequence of TFs.

To understand how Gcn4 mediates interaction with the NPC, we performed quantitative proteomics to identify proteins that interact with the PD_{GCN4}. The major nuclear export factor Crm1/Xpo1 binds Gcn4, and this interaction is weakened by mutations in the PD_{GCN4}. Single-molecule tracking of Crm1 suggests that ~12% of the protein is chromatin bound and, consistent with a previous study,[7] Crm1, Nup1, Nup2, and Nup60 bind upstream of hundreds of highly transcribed genes. Crm1 inhibition or depletion led to rapid loss of peripheral localization and Nup association genome-wide. Furthermore, inhibiting Crm1 or depleting Nup2 led to a strong global decrease in nascent transcription. *In vivo*, Crm1 interacts with the entire NPC and shows preferential interaction with Nup2. *In vitro*, Crm1 binds both Gcn4 and Nup2. Finally, the DNA binding activity of Gcn4 is stimulated by Crm1 and Ran-guanosine triphosphate (GTP), suggesting allosteric coupling between DNA binding and protein binding. We conclude that Crm1 is a critical adaptor for TF-mediated docking of DNA at the NPC.

RESULTS

Crm1/Xpo1 is required for localization of genes at the nuclear periphery

Mutations in the Gcn4 positioning domain disrupt Gcn4-mediated peripheral localization of *HIS4*.[29] To confirm that this is true for other Gcn4 targets, an array of 128 Lac operator binding sites (LacO array[33,34]) was introduced downstream of the Gcn4 target genes *HIS1*, *HIS2*, *HIS3*, and *HIS5* and at the *URA3* locus bearing a single copy of the Gcn4 binding site (*URA3:Gcn4BS*). GFP-tagged Lac repressor and a nuclear envelope membrane protein were expressed in these cells, and the co-localization of each locus with the nuclear envelope was measured using confocal microscopy.[12,33–35] All of these loci repositioned to the nuclear periphery upon histidine starvation in the wild-type strains but not in *gcn4-pd* strains (Figure 1A). Thus, mutations in the PD_{GCN4} disrupt peripheral localization of Gcn4 targets generally.

To identify proteins that interact with Gcn4 in a PD_{GCN4}-dependent manner, we immunopurified Gcn4-GFP from wild-type and *gcn4-pd* mutant strains grown in ^{14}N or ^{15}N-lysine medium, respectively.[36] Gcn4-GFP was recovered from each lysate using anti-GFP nanobody-coupled magnetic beads (LaG16[37]), and associated proteins were pooled and proteins were identified by tandem mass spectrometry (MS). Of 759 proteins identified (Table S1), only Crm1/Xpo1 was significantly enriched (2- to 3-fold) in two technical replicates (Figure 1B). Thus, Crm1 shows a PD_{GCN4}-sensitive interaction with Gcn4.

Crm1, the major nuclear export factor (exportin-1) in yeast, is a member of the karyopherin family of nucleocytoplasmic transport factors that interact with Phe-Gly (FG) repeat-containing Nups in the NPC to mediate trafficking of cargoes.[38,39] To test if Crm1 impacts Gcn4-mediated peripheral targeting, we utilized a yeast strain with the T539C mutation in Crm1, which renders it sensitive to the inhibitor leptomycin B (LMB[40]). LMB reacts covalently with C539 to block access to the nuclear export sequence (NES) binding pocket, causing an NLS-GFP-NES reporter to concentrate in the nucleus (Figure 1C). In this strain, *HIS1*, *HIS2*, *HIS3*, *HIS5*, and *URA3:Gcn4-BS* all lost peripheral localization in the presence of LMB (100 ng/mL, 30 min; Figure 1D). Thus, inhibiting Crm1 disrupts peripheral localization of Gcn4 target genes.

Crm1 inhibition also affected localization of non-Gcn4 targets. LMB led to loss of peripheral localization of four other genes: the inducible gene *INO1* and the constitutively expressed ribosomal protein genes *RPS0A*, *RPS1B*, and *RPS6A*[12,29] (Figure 1E). Peripheral localization was disrupted within 5–10 min of LMB addition (Figure 1F). Therefore, Crm1 inhibition rapidly disrupts peripheral localization of both Gcn4-dependent and Gcn4-independent genes.

We next asked if mutations in the positioning domain affected the nuclear localization of Gcn4. The nuclear-to-cytoplasmic ratio of wild-type Gcn4-GFP and gcn4-pd-GFP was indistinguishable (Figure S1A), suggesting that the PD_{GCN4} does not function as an NES. The function of Crm1 in peripheral localization of genes may be distinct from its role in nuclear export.

If Crm1 interacts with TFs *in vivo*, it should be associated with chromatin. Live-cell, single-molecule tracking (SMT)[41,42] of Crm1-Halo[43] stained with JFX554[44] revealed mostly highly diffusive molecules (Figures 1G and S1B). To estimate the range and number of dynamic states, we modeled the tracks in two ways: (1) using a non-parametric Bayesian state array (saSPT)[45,46] that accounts for experimental variations in localization and focus accuracy and (2) using the Spot-On displacement-based kinetic modeling.[47] The former captures aggregate behaviors by averaging across tracks, while the latter can categorize the diffusion behavior from short tracks (capturing the behaviors of particles that show more than one behavior during a track). Crm1-Halo tracks showed a range of diffusion coefficients (D_{coef}) from 0.002 to 3 $\mu m^2/s$ (Figure 1H). The fastest diffusing Crm1 (150 kDa) was slightly slower than free Halo (33 kDa), and we observed two slower diffusing states, one of which was slower than H2A.Z (i.e., chromatin; Figure 1H). The D_{coef} for this slow population ($\sim 10^{-2} \mu m/s$) is similar to that of chromatin interacting with the NPC.[48] Based on the distribution of Crm1 D_{coefs} (Figure 1H), we selected a three-state Spot-On model for Crm1 diffusion (computed from sets of three steps)

(G) Overlay of 24 individual Crm1-HALO tracks in a living cell (white oval), captured over a 30-s window and tracked at 100 Hz, colored according to diffusion coefficients. The nucleus is highlighted with the gold oval.
(H) Frequency histogram of Crm1, free HaloTag, and H2A.Z diffusivities from modeling.
(I) Kinetic modeling of displacement distances from 10- to 30-ms windows (data). The prediction from a three-state model (black line) is shown.
(J) Steady-state fractions of Crm1 exhibiting three distinct dynamic behaviors, estimated by kinetic modeling (H).

that showed excellent agreement with the data (Figure 1I). At steady state, ~12% of Crm1 molecules exhibit very slow diffusion (potentially chromatin-associated), and ~22% showed intermediate diffusion (Figure 1J; Table S2).

Crm1 and Nups bind upstream of hundreds of genes

Although Crm1 and Nups have been previously shown to interact with the yeast genome,[7] the precise location of these interactions was unclear. Therefore, we performed chromatin endogenous cleavage sequencing (ChEC-seq2[22,48,49]) to map Crm1, Nup1, Nup2, and Nup60 and the inner ring Nup157 association with the genome. Proteins were tagged with micrococcal nuclease (MNase),[50] a non-specific endonuclease that has an optimal calcium concentration of 10 mM[51] and is inactive *in vivo*. MNase digestion can be stimulated by briefly permeabilizing cells in the presence of 2 mM Ca^{+2}, and the cleavage sites can be mapped by next-generation sequencing.[49,52] The cleavage pattern is compared with cleavage by nuclear soluble MNase (sMNase) to control for non-specific cleavage of unprotected DNA.[49]

The Crm1, Nup1, Nup2, and Nup60 MNases cleaved the yeast genome significantly more than sMNase and showed similar cleavage patterns. At strongly transcribed genes like *TDH3*, Crm1, Nup1, Nup2, and Nup60 cleaved upstream of the promoter and within the upstream activating sequence (UAS) region (i.e., enhancers; Figure 2A). Cleavage by Nup157-MNase was quite weak. Metagene plots of average cleavage over all genes highlighted that Crm1, Nup1, Nup2, and Nup60 cleave upstream of the promoter (Figure S2A, top). To inspect the types of genes that interact with Nups and Crm1, we assessed cleavage over four categories of genes defined by their association with TFs and co-regulators[53]: (1) ribosomal protein genes (137 RPGs); (2) genes that interact with co-regulators such as the Spt/Ada/Gcn5 acetyltransferase (SAGA), the Tup1 repressor or Mediator (1,023 STM genes, inducible genes); (3) genes that interact with the pioneer factors Abf1 and Reb1 but do not recruit the STM co-regulators (1,549 transcription factor-only [TFO] genes); and (4) genes that interact with RNA polymerase II (RNAPII) but do not interact with known TFs or co-regulators (2,712 unbound [UNB] genes). The relative transcription levels of these genes are as follows: RPGs > STMs > TFO > UNB (Figure S2B). Crm1, Nup1, Nup2, and Nup60 association strongly resembled TF and co-regulator binding; cleavage by these proteins was apparent upstream of the RPGs, the STM genes, and the TFO genes but not upstream of the UNB genes (Figure 2B).

When the cleavage frequency by these proteins over upstream regions (−700 to −125) was compared with several negative controls (sMNase, the nucleosome binding protein Prp20 or histone H2A.Z[48]) by principal-component analysis, Crm1 and the Nups clustered separately from the control proteins (Figure 2C). Despite the very weak cleavage from Nup157, it clustered with the other Nups and Crm1. Thus, these proteins interact with a common set of enhancers and promoters.

To compare the occupancy of these proteins more precisely, we identified high-confidence cleavage sites using Double-ChEC.[48] Hundreds of high-confidence sites were identified for each of the Nups and thousands for Crm1 (Figure 2D). Thus, Crm1 associates with more locations than Nups. However, when the cleavage by each of the proteins was plotted over the sites identified for the other factors, we observed a high degree of cleavage of all sites by Crm1, Nup1, Nup2, and Nup60, but not sMNase (Figure 2D). Whereas the peaks identified by Nups showed comparable cleavage by Crm1, Nup1, Nup2, and Nup60, the peaks identified by Crm1 showed notably stronger cleavage by Crm1 (Figure 2D). This suggests that Crm1 interacts with Nup binding sites as well as other sites in the genome.

We also used ChEC-seq2 to examine inducible interaction with the NPC. Starving cells for amino acids caused an increase in cleavage by Crm1-MN and Nup2-MN at 627 high confidence Gcn4 binding sites[48] (Figure S2C, purple). This increase was not observed in *gcn4Δ* cells (Figure S2C, blue), confirming that Gcn4 is required for Crm1 and Nup2 recruitment to these sites.

Genes near the high confidence Nup/Crm1 sites were enriched for highly expressed metabolic enzyme genes and RPGs (Figure S2D; Table S3). These genes were compared with the genes bound to each of 78 different TFs.[53] Genes near high-confidence Crm1/Nup sites showed strong overlap with the targets of a small set of TFs (Figure S2E). The targets of three TFs consistently showed strong overlap with all of the genes near high-confidence Crm1/Nup sites: Abf1, Reb1, and Rap1 (Figure 2E). Indeed, motif discovery of DNA motifs enriched within the high-confidence Nup1 sites identified the binding sites for all of these TFs (Figures 2F and S2F). Crm1 sites were enriched for Rap1 (E value = 1.9 e−7) and Abf1 (E value = 1.3 e−3) sites, but not Reb1 sites.

We also assessed the overlap of the genes identified by ChEC with Crm1, Nup1, Nup2, and Nup60, as well as the overlap between each of these sets of genes with published targets of Nup157 and Nup170[56] or Mlp1[57] (Figures S2G and S2H). Although Crm1 associates with more genes than Nups, their targets strongly overlap; genes near Crm1 sites included 77% of the genes near Nup1 sites, 74% of the genes near Nup2 sites, and 96% of the genes near Nup60 sites. These genes also strongly overlap with Mlp1-associated genes (67%). However, the overlap with Nup157 and Nup170 was weaker (37% and 41%, respectively; Figures S2G and S2H).

Crm1 functions upstream of Nup2

To test if Crm1 bridges the interaction between TFs and the NPC, we asked if Crm1 is required for Nup2 association. For comparison, we also tested if Nup2 affects Crm1 binding to chromatin. We utilized either LMB-sensitive Crm1-T539C or auxin-inducible degron (AID[58]) alleles of Crm1 or Nup2. Nup2-AID was efficiently degraded upon addition of auxin (Figure S3A), disrupting peripheral localization of *INO1*, *RPS0A*, *RPS1B*, and *RPS6A*[29] (Figure 3A). Attempts to construct a Crm1-AID strain were unsuccessful, perhaps because of unfavorable interactions between the AID tag and Crm1 (modeled in Figure S3B). Therefore, we developed an alternative strategy to deplete Crm1-GFP (Figure S3B) by expression of a conditionally stable GFP binding protein (csGBP[59]) fused to the miniAID tag.[60] Inducing miniAID-csGBP and adding auxin (5-Ph-IAA) strongly inhibited growth of the Crm1-GFP strains (Figure S3C) and depleted Crm1-GFP (Figure S3D; we refer to this system as grAID for green fluorescence protein-mediated auxin-inducible degradation).

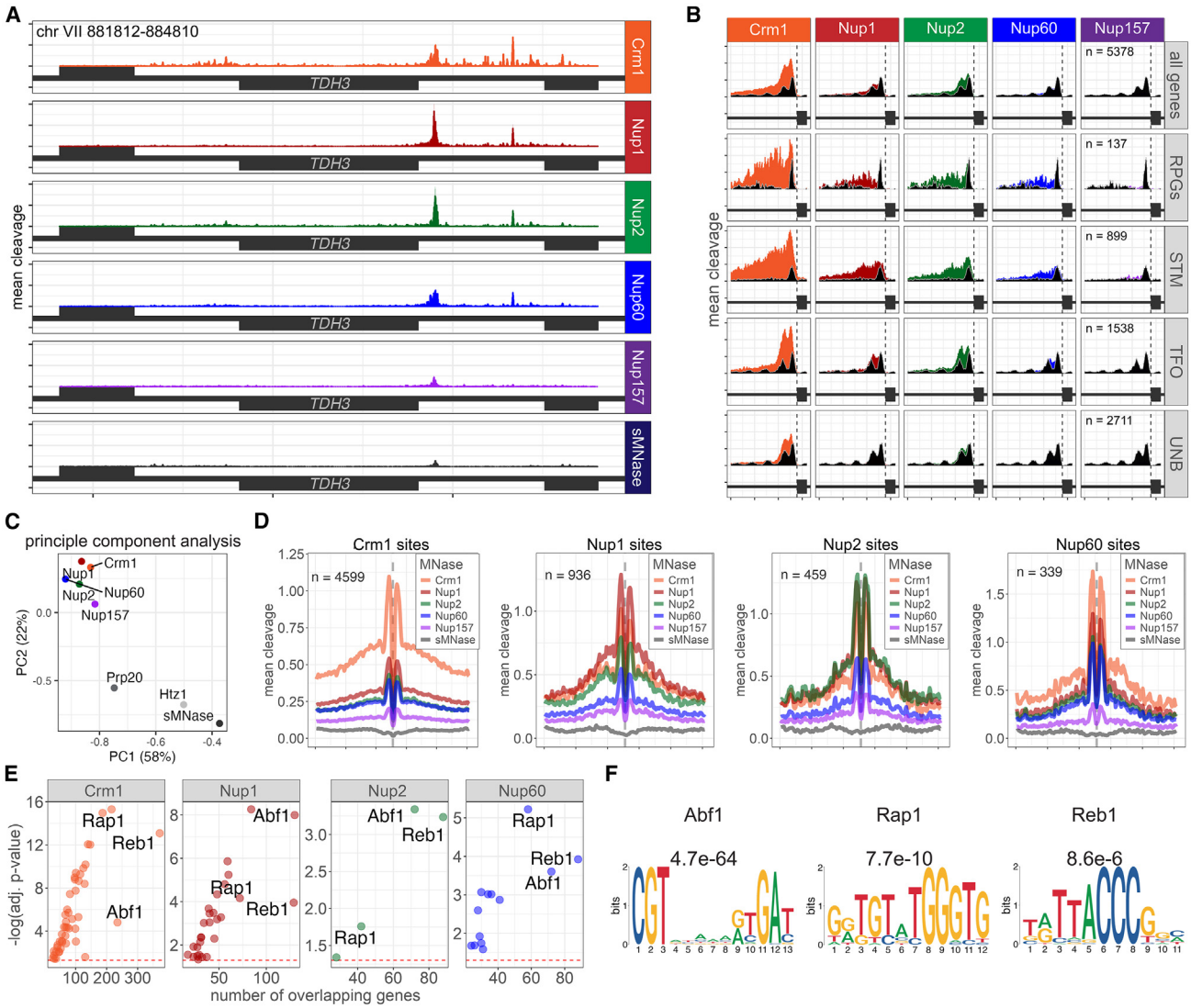

Figure 2. Crm1 and Nup association with the yeast genome

(A) Mean CPM-normalized ChEC-seq2 cleavage frequency of Crm1-MNase, Nup1-MNase, Nup2-MNase, Nup60-MNase, Nup157-MNase, and sMNase near the *TDH3* gene.

(B) Metagene plots of the average CPM-normalized ChEC cleavage 700 bp upstream and 200 bp downstream of the transcription start site (TSS) for all RNAPII transcribed genes or the indicated subsets.[53] Black: sMNase.

(C) Principal-component analysis of cleavage frequency 700 bp upstream of all genes by Crm1, Nup1, Nup60, Nup2, and Nup157 as well as controls (Prp20, sMNase, and H2A.Z[48]).

(D) Metasite plots of mean cleavage at high confidence Crm1, Nup1, Nup2, and Nup60 sites[48] ± 250 bp.

(E) Overlap between genes with near Crm1/Nups sites and TFs from ChIP-exo.[54,55] The number of overlapping genes was plotted against the Bonferroni-adjusted *p* value (Fisher's exact test).

(F) Top three MEME results from Nup1 peaks and respective E values.

Either depleting or inhibiting Crm1 led to decreased Nup2-MNase cleavage upstream of highly expressed genes and over Nup2 sites (Figures 3C–3E). The control proteins sMNase and Prp20 were unaffected by auxin treatment or Crm1 inhibition (Figures 3D and 3E). The effect of LMB on Nup2 ChEC was stronger than that of Crm1 depletion, perhaps because the grAID system leads to incomplete depletion of Crm1-GFP (Figure S3D). LMB inhibition blocked nuclear export but had no effect on the localization of Nup1, Nup2, or Nup60 (Figure 3B). Likewise, Crm1-MNase cleavage over enhancers and high confidence Crm1 sites was unaffected by Nup2 depletion (Figures 3C–3E). Therefore, Crm1 functions upstream of Nup2. Finally, because Nup2 depletion generally blocks targeting to the nuclear periphery[29] (Figure 3A), and because Crm1 localizes both in the nucleoplasm and at the nuclear periphery, we surmise Crm1 can interact with chromatin in the nucleoplasm.

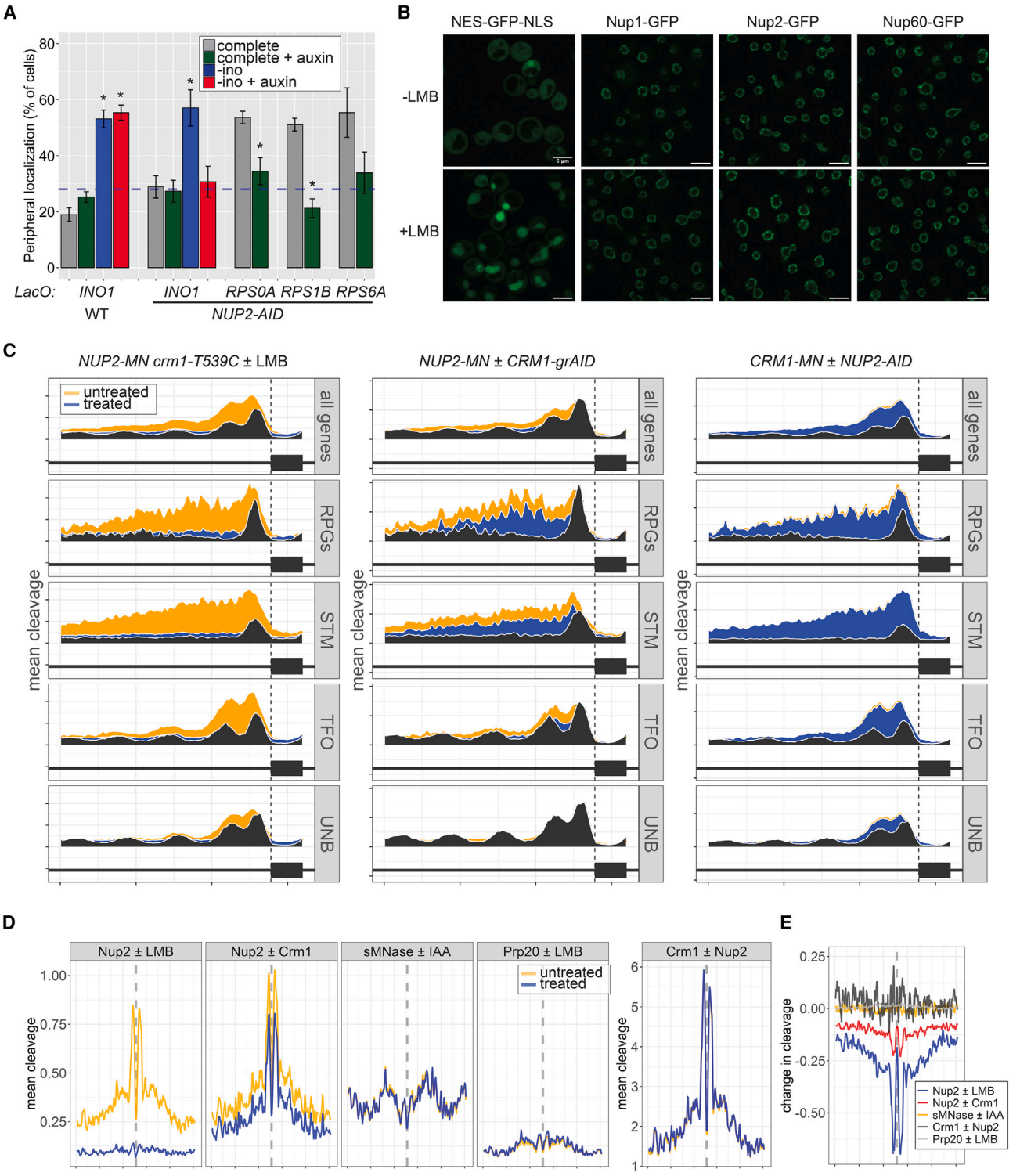

Figure 3. Crm1 functions upstream of Nup2

(A) Localization of *INO1*, *RPS0A*, *RPS1B*, and *RPS6A* in either a wild-type strain or a Nup2-AID strain ± 0.5mM auxin (IAA), 1 h. Asterisks indicate $p < 0.05$, compared with the untreated SDC control (Student's t test).

(B) Localization of GFP-tagged proteins in *crm1-T539C* ± LMB treatment.

(legend continued on next page)

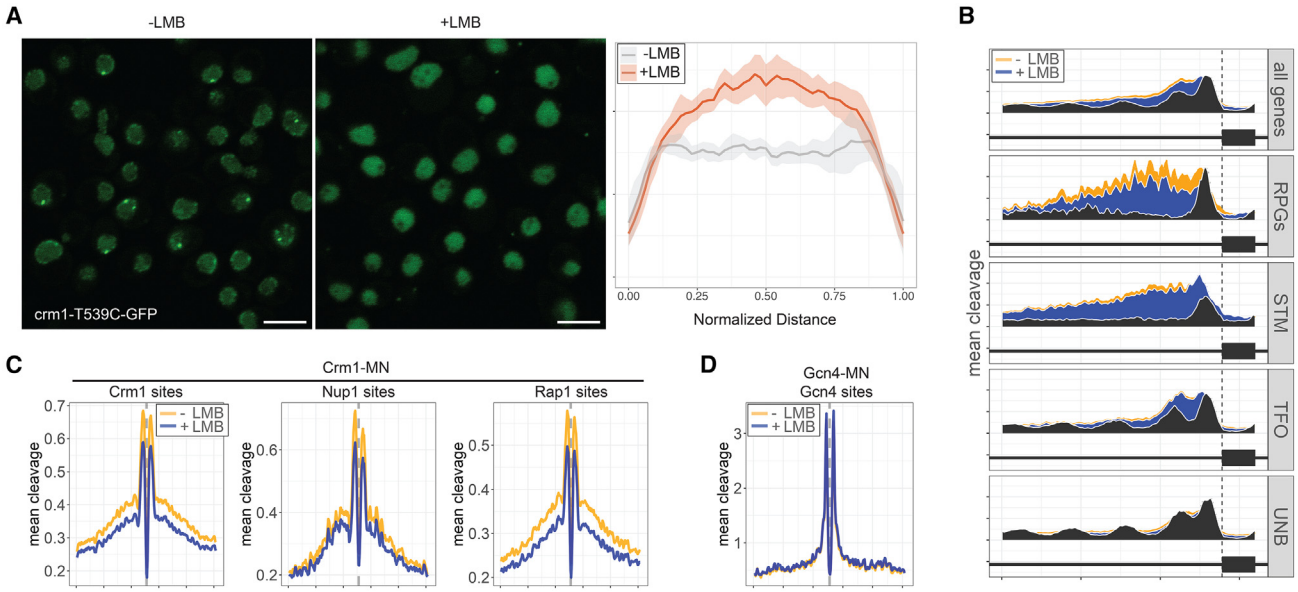

Figure 4. LMB alters Crm1 localization and chromatin interaction

(A) Localization of Crm1-T539C-GFP ± LMB treatment, imaged by confocal microscopy. Right: mean GFP intensity from line scans of 20 nuclei, with nuclear width normalized to 1.

(B and C) Cleavage by Crm1-T539C ± LMB. (B) Metagene plots (700 bp upstream and 200 bp downstream of the TSS) for subsets of genes with unique modes of RNAPII recruitment[53] and (C) mean Crm1 cleavage over high-confidence Crm1, Nup1, and Rap1 sites ± 250 bp.

(D) Average Gcn4 cleavage (± 250 bp flanking) over Gcn4 sites[48] ± 250 bp ± LMB.

LMB covalently modifies cysteine 539 within the NES binding site of Crm1,[40] suggesting that the NES binding site is important for chromatin-NPC interactions. To better understand the effects of LMB *in vivo*, we imaged Crm1-T539C-GFP and performed ChEC with Crm1-T539C-MNase ± LMB. LMB caused a dramatic relocalization of Crm1 from the nuclear periphery to the nucleoplasm (Figure 4A) and a global decrease in Crm1 association with chromatin (Figures 4B and 4C). This effect was specific to Crm1; cleavage by Gcn4-MNase near its binding sites was unaffected by LMB (Figure 4D). Crm1 mislocalization upon LMB treatment has also been seen in A549 cells[61] and *Xenopus*.[62] Thus, LMB may have unanticipated effects *in vivo* beyond blocking interaction with nuclear export cargo, leading to loss of Crm1-mediated NPC-chromatin interactions.

Crm1 and Nup2 promote transcription

Crm1 and Nups interact with highly expressed genes (Figure 2). In fact, ChEC-seq2 with RNAPII (Rpb1-MNase) revealed that the cleavage pattern of Rpb1-MNase upstream of all genes (-700 to +25 bp from the transcription start site) was strongly correlated with that of Crm1 and Nups (Spearman's rank correlation values of 0.71–0.95; Figure 5A). In contrast, Rpb1-MNase cleavage correlated poorly with that of sMNase (correlation = 0.14).

To test if the interaction of Crm1 and nuclear pore proteins like Nup2 promotes transcription, we measured total and nascent RNA using thiol (SH)-linked alkylation for the metabolic sequencing of RNA (SLAM-seq[63]) following inhibition of Crm1 with LMB or depletion of Nup2-AID. Both inhibition of Crm1 (30 min; Figure 5B) and depletion of Nup2-AID (16 h; Figure 5C) resulted in strong decreases in nascent mRNA levels. Depletion of Nup1 did not have this effect (Figure S4A). The genes downregulated by LMB inhibition of Crm1 or depletion of Nup2 overlapped strongly (Figure S4B), and the degree of downregulation correlated with the Crm1 and Nup2 occupancy (Figures S4D and S4E). This supports a role for Crm1 and Nup2 in promoting stronger transcription.

While the inhibition of Crm1 and depletion of Nup2 resulted in strong downregulation in nascent transcription of hundreds of genes, this decrease was not reflected in total mRNA levels (Figures 5B and 5C). This suggests that the defect associated with loss of Crm1 or Nups is strongly buffered through changes in mRNA half-life, a phenomenon that has been observed for perturbations that cause global defects in transcription.[64–67] Furthermore, the consequences of Nup2 depletion were not immediately apparent; after 1 h of Nup2 depletion, we observed no significant effect on nascent transcript levels (data not shown). Thus, while the effect of Crm1 inhibition was immediate, the effects of Nup2 depletion were only observed after several hours.

To test if decreased mRNA export upon inhibition of Crm1 or depletion of Nup2 could account for either the decrease in

(C–E) Mean cleavage by Crm1, Nup2, Prp20, or sMNase in strains either depleted of Nup2 (by Nup2-AID), depleted of Crm1 (using grAID), or inhibited with LMB (*crm1-T539C*). (C) Metagene plots 700 bp upstream and 200 bp downstream of the transcription start site of the indicated subsets of genes (previously described in Figure 2) ± LMB (left) or ± auxin (center and right). sMNase is in black. (D) Mean cleavage by the indicated proteins over high confidence Crm1 sites ± IAA (Crm1 ± Nup2) or Nup2 sites ±5-Ph-IAA and estradiol (Nup2 ± Crm1) or ± LMB. (E) Change in cleavage over the Nup2 sites upon each treatment.

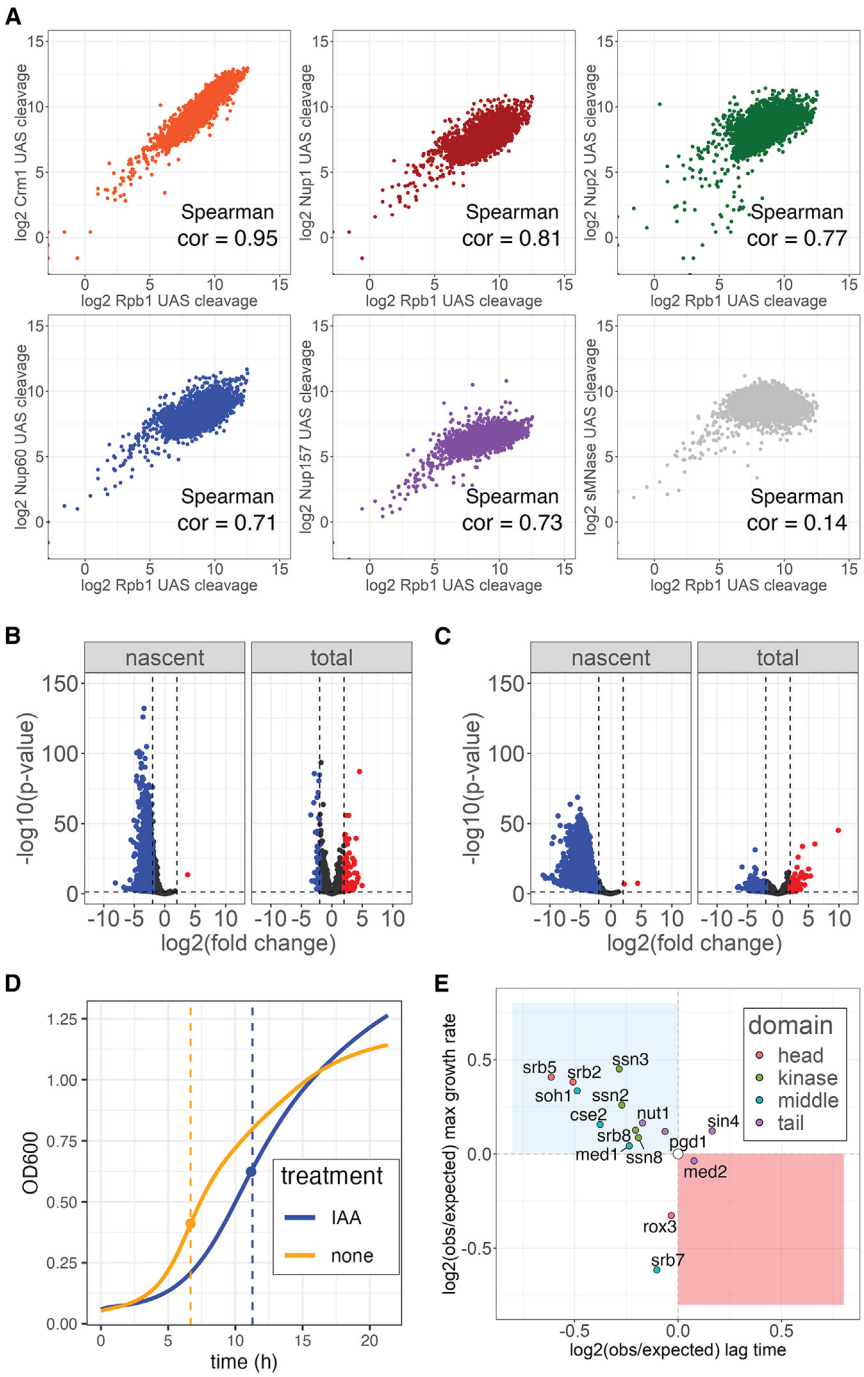

Figure 5. Crm1 and Nup2 promote stronger transcription

(A) Scatterplots and Spearman's correlation of Crm1 and Nup ChEC-seq2 cleavage vs. Rpb1-MNase cleavage −700 to −125 from transcriptional start site for all yeast genes.[32]

(B and C) SLAM-seq analysis of nascent and total mRNA from either a *crm1-T539C* strain ±LMB, 30 min (B) or a Nup2-AID strain ± auxin, 16 h (C).

(D) Growth analysis of Nup2-AID strain ± auxin. From the OD_{600} of cultures, the maximal growth rate (slope at the indicated time points) and the lag time (i.e., the time required to achieve the maximal growth rate) were determined (Table S4; STAR Methods). The ratio of the maximal growth rate and lag time for each double mutant was compared with the expected value obtained by multiplying the growth defects caused by each mutation.

(E) The white dot indicates the expected value for these parameters if the two mutations show additive phenotypes, while the blue and red squares indicate buffering and negative genetic interactions, respectively.

transcription or the longer mRNA half-lives in these mutants, we performed FISH against poly(A)+ mRNA in strains inhibited with LMB or depleted of Nup2 or the Mex67 mRNA exporter.[68] Inactivation of Mex67 led to a complete block in mRNA export (Figure S4F). Consistent with previous work,[69] inhibition of Crm1 with LMB perturbed mRNA export in a subset of cells, while depletion of Nup2 for 16 h had no effect (Figure S4F). Thus, the efficiency of mRNA export did not correlate with either decreases in nascent transcription or transcript buffering.

Disrupting the recruitment of genes to the nuclear periphery reduces the frequency of transcription,[25] suggesting that loss of interaction with the NPC impairs enhancer function.[70] We explored the relationship between Crm1/Nups and Mediator function by assessing genetic interactions between *NUP2* and each of the non-essential Mediator subunits. Null mutations for each of these subunits were introduced into Nup2-AID strains. For each strain, we measured the maximal growth rate ± auxin (Figure 5D, slope at the orange and blue dots, respectively) and the lag time required to reach that growth rate (dashed lines in Figure 5D). The fitness effect of loss of Nup2 is reflected in the increased lag and slower maximal growth rate in the presence of auxin (Figure 5D), and the fitness effect of each of the Mediator mutants was measured by comparing each *medΔ NUP2-AID* strain with the *NUP2-AID* strain without auxin (Table S4; STAR Methods). The fitness effect from loss of both Nup2 and a Mediator subunit was determined by measuring these parameters from the double-mutant strains + auxin.

Two mutations that affect unrelated biological functions should exhibit an additive fitness defect (white dot in Figure 5E), whereas two mutations that impact independent steps that contribute to the same biological function in parallel should produce a larger-than-expected effect on fitness (i.e., negative genetic interaction; red quadrant in Figure 5E). Finally, two mutations that impact the same step in a biological process should show

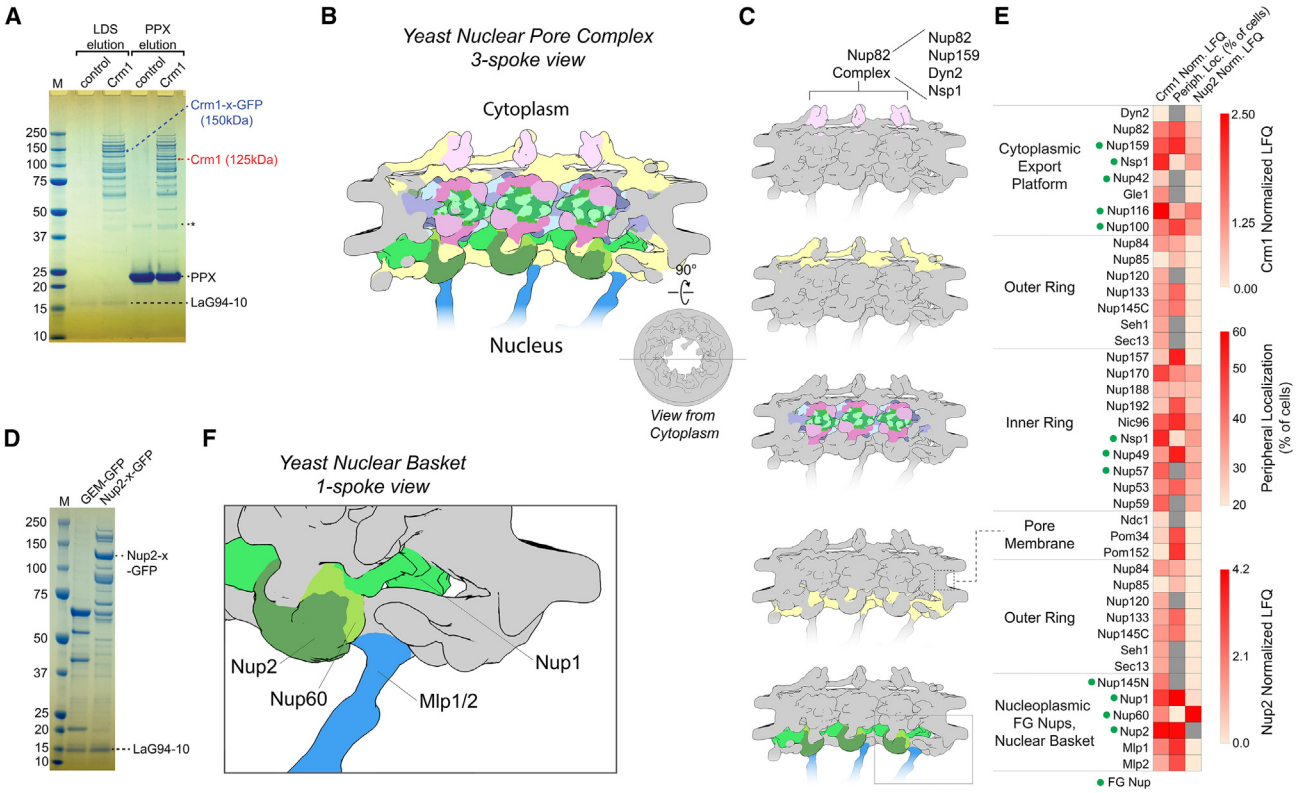

Figure 6. Crm1 and Nup2 interactions at the NPC overlap with the parts of the NPC that can contact chromatin

(A–C) Crm1-x-GFP (A) or Nup2-x-GFP (B) were purified from yeast using LaG94-10 α-GFP nanobody beads[37] and subjected to MS and label-free quantification. (A) Lanes 2 and 4 were from the Crm1-x-GFP strain; lanes 1 and 3 are a mock purification from a lysate lacking a GFP-tagged protein. Proteins were eluted by heating in LDS sample buffer (lanes 1 and 2) or by PreScission protease cleavage (PPX; lanes 3 and 4). (B and C) Yeast NPC structure (3-spoke view, B) and subcomplexes (C).

(D) Lane 1 is a control purification from a strain expressing genetically encoded multimeric particles tagged with GFP[76]; lane 2 is a purification from a strain expressing Nup2-x-GFP.

(E) Heatmap representing the normalized enrichment of each protein with Crm1 or Nup2, and peripheral localization (% of cells) of *URA3* induced by fusing LexA to each Nup in a strain having a LacO array and LexA BS at *URA3*[23,29] (Figure S5).

a less-than-additive "buffering" interaction because loss of either is equivalent to loss of both (blue quadrant in Figure 5E).[71] Mutations in most of the Mediator subunits exhibited buffering interactions with loss of Nup2 (Figures 5E and S5E). Specifically, three of the four middle domain subunits (red dots), two of the three kinase domain subunits (green dots), and two of the three head subunits (teal dots) showed buffering interactions. Tail subunits showed weak interactions (purple dots in Figure 5E). Two genes, *ROX3* and *SRB7*, showed more-than-additive decreases in maximal growth rate, but simple additive effects on lag phase (Figures 5E and S5E). These data suggest that Nup2 and Mediator impact the same process.

Crm1 interacts stably with the NPC

To identify molecular interactions that may be relevant to targeting of genes to the nuclear periphery, we purified Crm1 from yeast. Endogenous Crm1 was tagged with GFP downstream of a PreScission protease cleavage site (Crm1-x-GFP). Cells were lysed by cryomilling,[72] and Crm1-x-GFP was affinity-purified using magnetic beads coupled to the LaG94-10 anti-GFP nanobody[37] (Figure 6A). Crm1-x-GFP and several strong co-purifying bands were recovered with very little background (Figure 6A, lane 2 vs. 3). Cleavage by PreScission protease resulted in elution of these co-purifying proteins (Figure 6A, lanes 4 and 5), suggesting that they are bound to the beads through Crm1. The eluted material was concentrated, subjected to trypsin digestion and tandem MS, identifying 303 proteins, including every protein in the NPC (Table S5). Label-free quantification (LFQ) of these proteins revealed that the top 42 hits included all 36 subunits of the NPC and the transport factors Kap95, Srp1, Mex67, and Sac3 (Table S5). Normalizing to the stoichiometries of these proteins within the NPC[73] revealed a 10-fold range of intensities, presumably reflecting the strength of the interaction of Crm1 with NPC subcomplexes[74,75] (Figures 6B, 6C, and 6E). The strongest enrichments were from the RNA export platform (Nup159, Nup116, and Gle2), the inner ring (Nsp1, Nup57 and Nup170, and Nic96), and the nucleoplasmic FG repeat proteins Nup2 and Nup1 (Figure 6F). This suggests that Crm1 interacts stably with multiple parts of the NPC, including the nucleoplasmic face.

For comparison, we identified proteins that co-purified with Nup2-x-GFP (Figure 6D). As with Crm1, we identified all 32

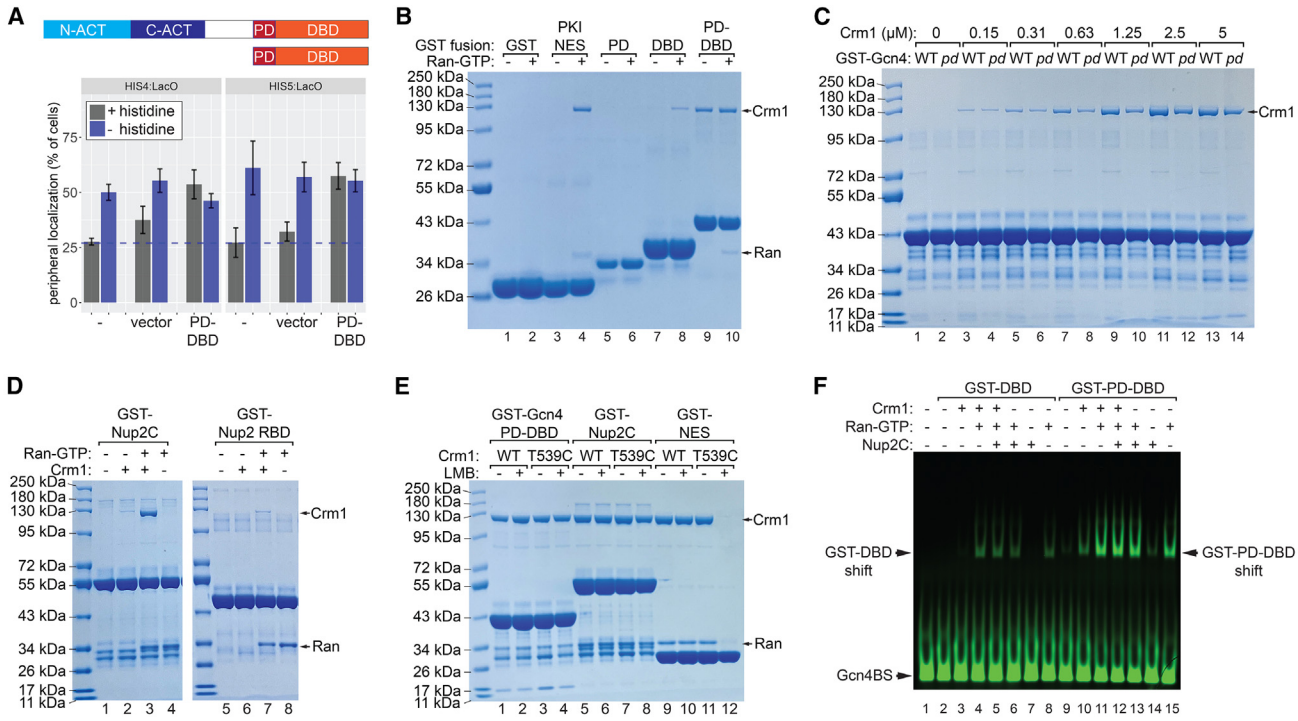

Figure 7. Crm1 binds to Gcn4 and Nup2

(A) Top: domains of Gcn4 and the PD-DBD fragment. Bottom: localization of *HIS4* and *HIS5* in strains transformed with the indicated constructs ± histidine. (B–E) GST fusion proteins on magnetic glutathione beads were incubated with different proteins, then the beads were washed, eluted with 40 mM glutathione, precipitated with trichloroacetic acid (TCA), and separated by SDS-PAGE. (B) GST pull-down with 2 μM Crm1 ± 2 μM H_6-Ran-GTP. (C) GST-PD-DBD (WT) or GST-*pd mutant*-DBD (*pd*) pull-down with the indicated concentrations of Crm1. (D) GST-Nup2C (left) or GST-Nup2-RBD (right) pull-down of 2.5 μM Crm1 ± 5 μM Ran-GTP. (E) GST-Gcn4-PD-DBD, GST-Nup2C, and GST-PKI NES pull-downs of either 2.5 μM Crm1-Ran-GTP (WT of T539C), ± 5 μM LMB. (F) EMSA of 20 pM fluorescent Gcn4 binding site incubated with 300 nM GST-DBD (lanes 2–8) or GST-PD-DBD (lanes 9–15) ± 1 μM Crm1, 1 μM Ran-GTP, or 1 μM Nup2C.

known NPC proteins (Table S5). However, normalization revealed a 400-fold range of intensities, suggesting that Nup2 shows a more specific interaction with the NPC than Crm1. Consistent with previous studies,[77–81] Nup2 interacted most strongly with Nup60 (Figures 6E and 6F[82]) and less strongly with the cytoplasmic export platform and the inner ring (Figure 6E).

We also asked which proteins in the NPC can contact chromatin. LexA was fused to the carboxyl terminus (C terminus) of 27 nuclear pore proteins. Into these strains, a LacO array ± the LexA binding site (LexA BS) at the *URA3* locus, GFP-LacI, and an ER/nuclear envelope membrane marker were introduced.[29] *URA3* normally localizes in the nucleoplasm, and we have used this strategy to test the effect of tethering TFs on nuclear positioning.[23,29] We reasoned that if LexA can come into contact with DNA, *URA3:LexABS* would localize at the nuclear periphery. Remarkably, over half of the Nups tested in this system were capable of repositioning *URA3* to the nuclear periphery in a LexA BS-dependent manner (Figure S5). Mapping these results onto the structure of the NPC showed a strong overlap between the Nups that were able to reposition chromatin to the nuclear periphery and those that interacted with Crm1 (Figure 6E). This suggests that the nucleoplasmic half of the NPC can contact chromatin, consistent with an open and flexible structure there.

Crm1 interacts directly with Gcn4 and Nup2

To test the hypothesis that Crm1 serves as an adaptor for TF-NPC interactions, we asked if Crm1 binds directly to either Gcn4 or Nup2. First, to identify a minimal portion of Gcn4 sufficient to mediate peripheral localization of Gcn4 target genes, we expressed 100 aa of the carboxyl terminal (C-terminal) portion of Gcn4 that includes both the PD_{GCN4} and the DNA binding domain (DBD) in yeast (PD-DBD; Figure 7A, top). Expressing this fragment caused both *HIS4* and *HIS5* to reposition constitutively to the nuclear periphery (Figure 7A), suggesting that this fragment recapitulates Gcn4-mediated targeting *in vivo*.

Purified, recombinant glutathione S-transferase (GST) fusion proteins bearing different fragments of Gcn4 or an NES from PKI[83] on glutathione magnetic beads were incubated with recombinant Crm1 ± His6-tagged Ran-GTP (Gsp1). As expected, the NES showed Ran-GTP-dependent binding to Crm1 (Figure 7B, lane 4). Crm1 failed to bind PD_{GCN4} alone, but it bound weakly to the DBD (lanes 7 and 8) and stronger to the PD-DBD (lanes 9 and 10). Curiously, while binding to the DBD was enhanced by Ran-GTP, binding to the PD-DBD was Ran-independent (lanes 9 and 10 and Figure S6A). Fluorescence polarization suggests that the Crm1-Gcn4 PD-DBD interaction has a K_D ~100 nM (Figure S6B). The *pd* mutations reduced the affinity of Crm1 for the PD-DBD (Figure 7C). Thus, Crm1 interacts with

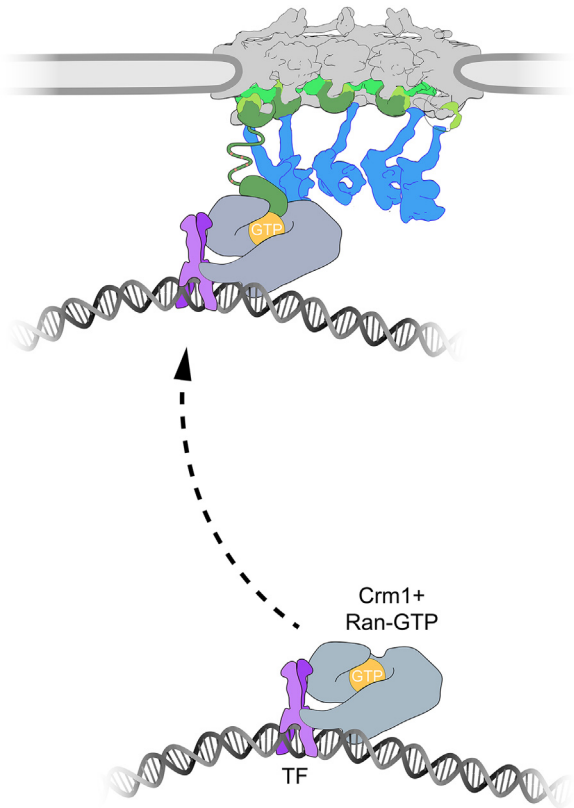

Figure 8. Model for Crm1 function as an adaptor for TF-NPC docking
Crm1-Ran-GTP associates with TFs bound to DNA in the nucleoplasm. The TF-Crm1-Ran complex undergoes random sub-diffusion in the nucleus.[87] When it encounters the NPC, it interacts with Nup2 (and potentially other Nups) to form a docking complex. This interaction could also occur with soluble Nups in the nucleoplasm, both in yeast and in other systems.

Gcn4 both through the DBD and the PD with distinct requirements for Ran-GTP. Alphafold3[84] predictions suggest that the PD_{GCN4} folds back on the DBD of the opposite member of the dimer, which could create a composite binding site (Figure S6C).

We hypothesized that Crm1 docks at the NPC through interaction with Nup2. Nup2 has a C-terminal Ran binding domain (RBD), which could interact with Crm1-Ran-GTP, and 12 FxFG repeats that could interact with the Crm1 surface HEAT repeats.[85,86] A similar complex has been reported between Crm1-Ran-GTP and Yrb2.[86] To test this model, we purified the C terminus of Nup2 (GST-Nup2C; aa 496–721, including two FxFGs and the RBD). For comparison, we also purified GST-Nup2-RBD (aa 583–721), lacking the FxFG repeats. Glutathione bead pull-downs showed weak binding of Crm1 to GST-Nup2C that was stimulated by Ran-GTP (Figure 7D, lanes 2 and 3). In contrast, GST-Nup2-RBD binding to Crm1 was only detected in the presence of Ran (Figure 7D, lanes 6 and 7), supporting the conclusion that Nup2 can interact with Crm1-Ran-GTP through both its FxFGs and its RBD.

To understand how LMB impacts these interactions, we tested the effects of LMB on interactions between Crm1 T539C-Ran-GTP and either Gcn4 PD-DBD, Nup2C or the PKI NES (Figure 7E). Wild-type Crm1 confirmed that there were no non-specific effects of LMB (lanes 2, 6, and 10). While LMB blocked the interaction of Crm1-T539C-Ran-GTP with GST-NES (lanes 11 and 12), it had no effect on the interaction with GST-PD-DBD (lanes 3 and 4) or GST-Nup2C (lanes 7 and 8). Thus, Crm1 binding to both Gcn4 and Nup2C occurs outside the NES binding pocket. Furthermore, Nup2C does not compete for binding of Crm1 to Gcn4 PD-DBD (Figure S6E). However, the interaction of Crm1-T539C-Ran-GTP with the Gcn4 DBD was reduced by LMB (Figure S6D). This suggests that while Crm1-Ran-GTP interacts with Nup2C and Gcn4 PD-DBD through surfaces distinct from the NES binding pocket, its interaction with the DBD is strengthened by the conformational changes stimulated by Ran-GTP and weakened by blocking the NES binding pocket.

Gcn4 and other TFs that mediate peripheral localization do not visibly concentrate at the nuclear periphery. If Crm1 and/or Nup2 interacts preferentially with DNA-bound TFs, this could facilitate docking of DNA-bound TFs at the NPC. We tested this idea by adding Crm1, His6-Ran-GTP, or Nup2C to GST-DBD or GST-PD-DBD in an electrophoretic mobility shift assay (EMSA) with fluorescently labeled Gcn4 binding site (Figure 7F). Using a concentration of Gcn4 that results in shifting of a small fraction of the probe (lane 9), DNA binding by the PD-DBD was enhanced by Crm1 alone (lane 10) or Ran-GTP alone (lane 15) but most strongly by Crm1 + Ran-GTP (lane 11). Consistent with this effect of Ran-GTP alone, we observed a weak interaction of Ran-GTP with GST-PD-DBD (Figure S6G, lane 10). Nup2 had no effect on DNA binding (Figure 7F, lane 14). The stimulation of DNA binding by Crm1-Ran-GTP was unaffected by the *pd* mutation (Figure S6F) and was also observed for the DBD alone, albeit less strongly (Figure 7F, lanes 4 and 8). The mobility of the shifted species was the same as that observed in the absence of Crm1 (e.g., lane 9 vs. 10), suggesting that it is a Gcn4-DNA complex. Thus, Crm1 and Ran-GTP stimulate DNA binding by Gcn4.

DISCUSSION

We propose that Crm1 serves as an adaptor between TFs and nuclear pore proteins to mediate chromatin-NPC interactions and promote transcription (Figure 8). This function is distinct from Crm1's role as a nuclear export factor; Crm1 binding to Gcn4 PD-DBD is Ran-GTP independent and is unaffected by covalent modification of the NES binding pocket by LMB. Thus, we propose that Gcn4 (and potentially other TFs) binds to a different surface of Crm1. Crm1-Ran-GTP bound to TFs on chromatin could undergo random sub-diffusion until they encounter the NPC,[87] where they form a complex with Nup2 (and potentially other Nups). The affinity of the Crm1-Gcn4 interaction (~100 nM) is consistent with 12% of Crm1 associated with chromatin and with the transient, continuous targeting to the nuclear periphery observed in live-cell tracking experiments.[87] Although the Crm1 binding to PD-DBD does not require Ran-GTP, Ran-GTP likely plays an important role. Both the interaction of Crm1 with the Gcn4 DBD and the interaction of Crm1 with Nup2C are stimulated by Ran-GTP, as is the interaction of Nup2 with Nup60 on the NPC.[79] Likewise, both Crm1 and Ran-GTP enhance the DNA binding by Gcn4. Thus, *in vivo*, Crm1-Ran-GTP is the likely link between TFs bound to chromatin and the NPC (Figure 8).

Inhibiting Crm1 with LMB or depletion by grAID leads to a global loss of Nup2 association and loss of peripheral localization of both Gcn4 targets and non-Gcn4 targets. This suggests that many TFs rely on Crm1 to mediate interaction with the NPC. If so, then other TFs should also have positioning domains that are necessary and sufficient to mediate peripheral localization. While the PD_{GCN4} is highly conserved among Gcn4 homologs in fungi, we have not identified such sequence motifs in other yeast TFs. Different TFs may interact with different surfaces on Crm1, so they may have functionally equivalent domains with dissimilar sequences. This is akin to the relationship between the amino acid sequence and function of transcriptional activation domains (acidic [Gcn4, VP16], proline-rich [AP-2], glutamine-rich [Sp1], serine/threonine-rich [nuclear factor κB (NF-κB)]). These domains all function to recruit co-activators and Mediator[88] but lack aa sequence identity.

Both depletion and inhibition of Crm1 perturb the association of Nup2 with chromatin. LMB inhibits Crm1 by blocking binding to NESs.[40] It is surprising that LMB impacts interaction of chromatin with the NPC since Crm1 binding to Gcn4 is mechanistically distinct from Crm1 binding to NESs. However, LMB also causes mislocalization of Crm1 in yeast (Figure 4A), A549 cells,[61] and *X. laevis*.[62] Also, while LMB had no effect on the interaction of Crm1-Ran-GTP with Nup2C or Gcn4-PD-DBD, it did impact binding to Gcn4 DBD (Figure S6D). Thus, LMB may have broader effects on Crm1 beyond blocking NES binding.

Based on Crm1 and Nup co-occupancy with RNAPII, genetic interactions of *NUP2* with Mediator, and strong global defects in nascent transcription upon inhibition of Crm1 or Nup2, we conclude that the interaction with these factors promotes transcription of hundreds of yeast genes. While the effect of Crm1 on transcription was very rapid (within 30 min), the effect of Nup2 degradation was slow, requiring several hours. This suggests that Crm1 has a more direct role than Nup2. Because depletion of Nup2 leads to rapid loss of peripheral localization,[29] we conclude that Crm1 binding, rather than localization at the nuclear periphery per se, promotes transcription. Consistent with this notion, Crm1 binds to many sites in the genome that do not interact well with Nups, raising the possibility that these sites may localize in the nucleoplasm but rely on Crm1 for maximal transcription.

How does Crm1 impact transcription? Crm1 may promote stronger transcription both by strengthening TF binding to DNA to increase occupancy and by facilitating recruitment of Nups. FG Nups are mostly unstructured proteins that physically interact with histone-modifying enzymes.[89–93] Thus, Nups may facilitate histone modifications and/or enhance the formation of phase-separated condensates that promote transcription.[94] Indeed, tethering Nup153 to chromatin promotes the formation of phase-separated foci that include RNAPII and Mediator.[95] Nups, together with Mediator, could thereby strengthen enhancer function to promote burst frequency. Consistent with this idea, the Gcn4 *pd* mutation destabilizes RNAPII associated with promoters of Gcn4 target genes.[32]

Limitations of the study

While our biochemical and genetic experiments strongly suggest that Crm1 plays distinct roles in nuclear export and chromatin localization, the best test of this model will be separation-of-function mutations in Crm1 that block either of these functions but not both. Future work will test if Crm1 serves as an adaptor for other TFs in yeast and other organisms. It seems plausible that Crm1 has a similar role in mammals. In certain leukemias, Crm1 co-occupies the *HOX* locus with the leukemogenic fusion proteins such as NUP98-HOXA9 or SET-NUP214 or mutant NPM1, and inhibiting Crm1 releases these proteins.[96–98] Likewise, fusion of Crm1 to the histone methyltransferase AFT10/MLLT10 drives leukemia by upregulating expression of the *HOXA/B* gene cluster expression,[99] presumably because Crm1 is recruited strongly to this locus in stem cells.[97] Understanding how Crm1 and Nups impact transcription, silencing, and epigenetic poising will also be important future challenges.

RESOURCE AVAILABILITY

Lead contact

Further information should be directed to and will be fulfilled by the lead contact, Jason H. Brickner (j-brickner@northwestern.edu).

Materials availability

All unique/stable reagents generated in this study are available from the lead contact with a completed materials transfer agreement.

Data and code availability

- All data reported in this paper have been deposited to Gene Expression Omnibus accession number GEO: GSE288820 and processed data to Mendeley Data (https://doi.org/10.17632/kjym3w4g36.1).
- ChEC-seq2 and SLAM-seq datasets generated in this study are publicly available under accession numbers GEO: GSE288515, GSE288549, and GSE288550 (ChEC-seq2) and GSE288633 (SLAM-seq). Metadata for individual files are provided in Table S7.
- This work did not generate any new code. Any additional information required to reanalyze the data reported in this paper is available from the lead contact upon request.

ACKNOWLEDGMENTS

The authors thank Professor Eric Weiss (Northwestern) for sharing the *crm1-T539C* strains, Professor Reza Vafabakhsh (Northwestern) for sharing nanobody-coupled beads, Winny Liu for help with plasmid construction, Dr. Atsushi Satomura for help developing SLAM-seq and ChEC-seq2, Dr. Trevor Van Eeuwen (Rockefeller) for help with figures, and members of the Brickner laboratory for helpful comments on the manuscript. This work was supported by NIH grants R35GM136419 (J.H.B.), P41 GM109824 (M.P.R. and B.C.), R01 GM112108 (M.P.R.), T32 NIGMS GM008061 (T.G. and D.J.V.), and F32 GM153164 (C.C.) and a predoctoral fellowship from the National Science Foundation (D.J.V.).

AUTHOR CONTRIBUTIONS

J.H.B. conceptualized and supervised the study. D.G.B. and S.U. performed gene localization and time-course experiments. J.H.B. performed SILAC-MS. T.G., G.C.M., and V.Q.N. designed and tested Crm1-HALO single-molecule tracking. G.C.M. and V.Q.N. computed displacement distances and performed kinetic modeling. T.G., D.G.B., and D.J.V. performed ChEC-seq2 experiments. J.H.B. analyzed ChEC-seq2 data. T.G. conceptualized and tested Crm1-grAID strains and Nup2-AID mediator knockout strains. D.G.B. performed poly(A)+ RNA FISH. J.H.B., W.Z., C.C., B.C., and M.P.R. designed and performed MS with label-free quantification. C.C. and M.P.R. visualized NPC structure and mapping. D.G.B. designed and tested peripheral localization of LexA-tagged nuclear pore proteins. T.G. and N.M. performed SLAM-seq. T.G. and A.J. localized and quantified Nups and Crm1 localization. J.H.B. and K.Z.

purified proteins and performed GST pull-downs, EMSAs, and fluorescence polarization assays. J.H.B. and T.G. performed formal statistical analysis. J.H.B. and T.G. wrote the manuscript. All authors reviewed and edited the manuscript. J.H.B. managed project administration and funding acquisition.

DECLARATION OF INTERESTS

The authors declare no competing interests.

STAR★METHODS

Detailed methods are provided in the online version of this paper and include the following:

- KEY RESOURCES TABLE
- EXPERIMENTAL MODEL AND STUDY PARTICIPANT DETAILS
- METHOD DETAILS
  - Chemicals, media and growth conditions
  - Yeast strains, plasmids, and molecular biology
  - Microscopy
  - Live-cell, single-molecule tracking
  - Stable Isotope Labelling by Amino acids in Cell culture (SILAC) mass spectrometry
  - Purification of Crm1-x-GFP and Nup2-x-GFP
  - ChEC seq2 and SLAM-seq and data analysis
  - Nup2-Mediator genetic interactions
  - grAID (green fluorescent protein-targeted AID)
  - Protein purification and labeling
  - GST pulldown experiments
  - Electrophoretic Mobility Shift Assay
- QUANTIFICATION AND STATISTICAL ANALYSIS

SUPPLEMENTAL INFORMATION

Supplemental information can be found online at https://doi.org/10.1016/j.molcel.2025.02.013.

Received: June 10, 2024
Revised: December 16, 2024
Accepted: February 14, 2025
Published: March 10, 2025

REFERENCES

1. Lin, D.H., and Hoelz, A. (2019). The Structure of the Nuclear Pore Complex (An Update). Annu. Rev. Biochem. *88*, 725–783. https://doi.org/10.1146/annurev-biochem-062917-011901.
2. Akey, C.W., Singh, D., Ouch, C., Echeverria, I., Nudelman, I., Varberg, J.M., Yu, Z., Fang, F., Shi, Y., Wang, J., et al. (2022). Comprehensive structure and functional adaptations of the yeast nuclear pore complex. Cell *185*, 361–378.e25. https://doi.org/10.1016/j.cell.2021.12.015.
3. Dultz, E., Wojtynek, M., Medalia, O., and Onischenko, E. (2022). The Nuclear Pore Complex: Birth, Life, and Death of a Cellular Behemoth. Cells *11*, 1456. https://doi.org/10.3390/cells11091456.
4. Gozalo, A., Duke, A., Lan, Y., Pascual-Garcia, P., Talamas, J.A., Nguyen, S.C., Shah, P.P., Jain, R., Joyce, E.F., and Capelson, M. (2020). Core Components of the Nuclear Pore Bind Distinct States of Chromatin and Contribute to Polycomb Repression. Mol. Cell *77*, 67–81.e7. https://doi.org/10.1016/j.molcel.2019.10.017.
5. de Van de Vosse, D.W.V., Wan, Y., Wozniak, R.W., and Aitchison, J.D. (2011). Role of the nuclear envelope in genome organization and gene expression. Wiley Interdiscip. Rev. Syst. Biol. Med. *3*, 147–166. https://doi.org/10.1002/wsbm.101.
6. Casolari, J.M., Brown, C.R., Drubin, D.A., Rando, O.J., and Silver, P.A. (2005). Developmentally induced changes in transcriptional program alter spatial organization across chromosomes. Genes Dev. *19*, 1188–1198.
7. Casolari, J.M., Brown, C.R., Komili, S., West, J., Hieronymus, H., and Silver, P.A. (2004). Genome-wide localization of the nuclear transport machinery couples transcriptional status and nuclear organization. Cell *117*, 427–439.
8. Kalverda, B., Pickersgill, H., Shloma, V.V., and Fornerod, M. (2010). Nucleoporins directly stimulate expression of developmental and cell-cycle genes inside the nucleoplasm. Cell *140*, 360–371. https://doi.org/10.1016/j.cell.2010.01.011.
9. Liang, Y., Franks, T.M., Marchetto, M.C., Gage, F.H., and Hetzer, M.W. (2013). Dynamic Association of NUP98 with the Human Genome. PLoS Genet. *9*, e1003308. https://doi.org/10.1371/journal.pgen.1003308.
10. Capelson, M., Liang, Y., Schulte, R., Mair, W., Wagner, U., and Hetzer, M.W. (2010). Chromatin-bound nuclear pore components regulate gene expression in higher eukaryotes. Cell *140*, 372–383. https://doi.org/10.1016/j.cell.2009.12.054.
11. Shokrollahi, M., Stanic, M., Hundal, A., Chan, J.N.Y., Urman, D., Jordan, C.A., Hakem, A., Espin, R., Hao, J., Krishnan, R., et al. (2024). DNA double-strand break–capturing nuclear envelope tubules drive DNA repair. Nat. Struct. Mol. Biol. *31*, 1319–1330. https://doi.org/10.1038/s41594-024-01286-7.
12. Brickner, J.H., and Walter, P. (2004). Gene Recruitment of the Activated INO1 Locus to the Nuclear Membrane. PLoS Biol. *2*, e342. https://doi.org/10.1371/journal.pbio.0020342.
13. Brickner, D.G., Cajigas, I., Fondufe-Mittendorf, Y., Ahmed, S., Lee, P.-C., Widom, J., and Brickner, J.H. (2007). H2A.Z-Mediated Localization of Genes at the Nuclear Periphery Confers Epigenetic Memory of Previous Transcriptional State. PLoS Biol. *5*, e81. https://doi.org/10.1371/journal.pbio.0050081.
14. Ahmed, S., Brickner, D.G., Light, W.H., Cajigas, I., McDonough, M., Froyshteter, A.B., Volpe, T., and Brickner, J.H. (2010). DNA zip codes control an ancient mechanism for gene targeting to the nuclear periphery. Nat. Cell Biol. *12*, 111–118. https://doi.org/10.1038/ncb2011.
15. Choudhry, S.K., Neal, M.L., Li, S., Navare, A.T., Van Eeuwen, T.V., Wozniak, R.W., Mast, F.D., Rout, M.P., and Aitchison, J.D. (2023). Nuclear pore complexes mediate subtelomeric gene silencing by regulating PCNA levels on chromatin. J. Cell Biol. *222*, e202207060. https://doi.org/10.1083/jcb.202207060.
16. Kadota, S., Ou, J., Shi, Y., Lee, J.T., Sun, J., and Yildirim, E. (2020). Nucleoporin 153 links nuclear pore complex to chromatin architecture by mediating CTCF and cohesin binding. Nat. Commun. *11*, 2606. https://doi.org/10.1038/s41467-020-16394-3.
17. Taddei, A., Van Houwe, G.V., Hediger, F., Kalck, V., Cubizolles, F., Schober, H., and Gasser, S.M. (2006). Nuclear pore association confers optimal expression levels for an inducible yeast gene. Nature *441*, 774–778. https://doi.org/10.1038/nature04845.
18. Nagai, S., Dubrana, K., Tsai-Pflugfelder, M., Davidson, M.B., Roberts, T.M., Brown, G.W., Varela, E., Hediger, F., Gasser, S.M., and Krogan, N.J. (2008). Functional targeting of DNA damage to a nuclear pore-associated SUMO-dependent ubiquitin ligase. Science *322*, 597–602. https://doi.org/10.1126/science.1162790.
19. Jacinto, F.V., Benner, C., and Hetzer, M.W. (2015). The nucleoporin Nup153 regulates embryonic stem cell pluripotency through gene silencing. Genes Dev. *29*, 1224–1238. https://doi.org/10.1101/gad.260919.115.
20. Light, W.H., Brickner, D.G., Brand, V.R., and Brickner, J.H. (2010). Interaction of a DNA Zip Code with the Nuclear Pore Complex Promotes H2A.Z Incorporation and INO1 Transcriptional Memory. Mol. Cell *40*, 112–125. https://doi.org/10.1016/j.molcel.2010.09.007.
21. Cabal, G.G., Genovesio, A., Rodriguez-Navarro, S., Zimmer, C., Gadal, O., Lesne, A., Buc, H., Feuerbach-Fournier, F., Olivo-Marin, J.C., Hurt,

E.C., et al. (2006). SAGA interacting factors confine sub-diffusion of transcribed genes to the nuclear envelope. Nature *441*, 770–773.

22. Schmid, M., Arib, G., Laemmli, C., Nishikawa, J., Durussel, T., and Laemmli, U.K. (2006). Nup-PI: The Nucleopore-Promoter Interaction of Genes in Yeast. Mol. Cell *21*, 379–391. https://doi.org/10.1016/j.molcel.2005.12.012.
23. Randise-Hinchliff, C., Coukos, R., Sood, V., Sumner, M.C., Zdraljevic, S., Meldi Sholl, L., Garvey Brickner, D., Ahmed, S., Watchmaker, L., and Brickner, J.H. (2016). Strategies to regulate transcription factor-mediated gene positioning and interchromosomal clustering at the nuclear periphery. J. Cell Biol. *212*, 633–646. https://doi.org/10.1083/jcb.201508068.
24. Brickner, D.G., Ahmed, S., Meldi, L., Thompson, A., Light, W., Young, M., Hickman, T.L., Chu, F., Fabre, E., and Brickner, J.H. (2012). Transcription Factor Binding to a DNA Zip Code Controls Interchromosomal Clustering at the Nuclear Periphery. Dev. Cell *22*, 1234–1246. https://doi.org/10.1016/j.devcel.2012.03.012.
25. Brickner, D.G., Sood, V., Tutucci, E., Coukos, R., Viets, K., Singer, R.H., and Brickner, J.H. (2016). Subnuclear positioning and interchromosomal clustering of the GAL1-10 locus are controlled by separable, interdependent mechanisms. Mol. Biol. Cell *27*, 2980–2993. https://doi.org/10.1091/mbc.E16-03-0174.
26. Zhu, X., Qi, C., Wang, R., Lee, J.-H., Shao, J., Bei, L., Xiong, F., Nguyen, P.T., Li, G., Krakowiak, J., et al. (2022). Acute depletion of human core nucleoporin reveals direct roles in transcription control but dispensability for 3D genome organization. Cell Rep. *41*, 111576. https://doi.org/10.1016/j.celrep.2022.111576.
27. Huang, P., Zhang, X., Cheng, Z., Wang, X., Miao, Y., Huang, G., Fu, Y.-F., and Feng, X. (2024). The nuclear pore Y-complex functions as a platform for transcriptional regulation of FLOWERING LOCUS C in Arabidopsis. Plant Cell *36*, 346–366. https://doi.org/10.1093/plcell/koad271.
28. D'Urso, A., Takahashi, Y.-H., Xiong, B., Marone, J., Coukos, R., Randise-Hinchliff, C., Wang, J.-P., Shilatifard, A., and Brickner, J.H. (2016). Set1/COMPASS and Mediator are repurposed to promote epigenetic transcriptional memory. eLife *5*, e16691. https://doi.org/10.7554/eLife.16691.
29. Brickner, D.G., Randise-Hinchliff, C., Lebrun Corbin, M.L., Liang, J.M., Kim, S., Sump, B., D'Urso, A., Kim, S.H., Satomura, A., Schmit, H., et al. (2019). The role of transcription factors and nuclear pore proteins in controlling the spatial organization of the yeast genome. Dev. Cell *49*, 936–947.e4. https://doi.org/10.1016/j.devcel.2019.05.023.
30. Ibarra, A., Benner, C., Tyagi, S., Cool, J., and Hetzer, M.W. (2016). Nucleoporin-mediated regulation of cell identity genes. Genes Dev. *30*, 2253–2258. https://doi.org/10.1101/gad.287417.116.
31. Hope, I.A., and Struhl, K. (1986). Functional dissection of a eukaryotic transcriptional activator protein, GCN4 of yeast. Cell *46*, 885–894.
32. VanBelzen, J., Sakelaris, B., Brickner, D.G., Marcou, N., Riecke, H., Mangan, N.M., and Brickner, J.H. (2024). Chromatin endogenous cleavage provides a global view of yeast RNA polymerase II transcription kinetics. eLife *13*, RP100764. https://doi.org/10.7554/eLife.100764.
33. Robinett, C.C., Straight, A., Li, G., Willhelm, C., Sudlow, G., Murray, A., and Belmont, A.S. (1996). In vivo localization of DNA sequences and visualization of large-scale chromatin organization using lac operator/repressor recognition. J. Cell Biol. *135*, 1685–1700.
34. Straight, A.F., Belmont, A.S., Robinett, C.C., and Murray, A.W. (1996). GFP tagging of budding yeast chromosomes reveals that protein-protein interactions can mediate sister chromatid cohesion. Curr. Biol. *6*, 1599–1608.
35. Egecioglu, D.E., D'Urso, A., Brickner, D.G., Light, W.H., and Brickner, J.H. (2014). Approaches to Studying Subnuclear Organization and Gene–Nuclear Pore Interactions. Chapter 21. In Methods in Cell Biology, *122* (Elsevier), pp. 463–485. https://doi.org/10.1016/B978-0-12-417160-2.00021-7.
36. Ong, S.-E., Blagoev, B., Kratchmarova, I., Kristensen, D.B., Steen, H., Pandey, A., and Mann, M. (2002). Stable Isotope Labeling by Amino Acids in Cell Culture, SILAC, as a Simple and Accurate Approach to Expression Proteomics. Mol. Cell. Proteomics *1*, 376–386. https://doi.org/10.1074/mcp.m200025-mcp200.
37. Fridy, P.C., Li, Y., Keegan, S., Thompson, M.K., Nudelman, I., Scheid, J.F., Oeffinger, M., Nussenzweig, M.C., Fenyö, D., Chait, B.T., et al. (2014). A robust pipeline for rapid production of versatile nanobody repertoires. Nat. Methods *11*, 1253–1260. https://doi.org/10.1038/nmeth.3170.
38. Lusk, C.P., Makhnevych, T., Marelli, M., Aitchison, J.D., and Wozniak, R.W. (2002). Karyopherins in nuclear pore biogenesis: a role for Kap121p in the assembly of Nup53p into nuclear pore complexes. J. Cell Biol. *159*, 267–278. https://doi.org/10.1083/jcb.200203079.
39. Aramburu, I.V., and Lemke, E.A. (2017). Floppy but not sloppy: interaction mechanism of FG-nucleoporins and nuclear transport receptors. Semin. Cell Dev. Biol. *68*, 34–41. https://doi.org/10.1016/j.semcdb.2017.06.026.
40. Kudo, N., Matsumori, N., Taoka, H., Fujiwara, D., Schreiner, E.P., Wolff, B., Yoshida, M., and Horinouchi, S. (1999). Leptomycin B inactivates CRM1/exportin 1 by covalent modification at a cysteine residue in the central conserved region. Proc. Natl. Acad. Sci. USA *96*, 9112–9117. https://doi.org/10.1073/pnas.96.16.9112.
41. Nguyen, V.Q., Ranjan, A., Liu, S., Tang, X., Ling, Y.H., Wisniewski, J., Mizuguchi, G., Li, K.Y., Jou, V., Zheng, Q., et al. (2021). Spatiotemporal coordination of transcription preinitiation complex assembly in live cells. Mol. Cell *81*, 3560–3575.e6. https://doi.org/10.1016/j.molcel.2021.07.022.
42. Lionnet, T., and Wu, C. (2021). Single-molecule tracking of transcription protein dynamics in living cells: seeing is believing, but what are we seeing? Curr. Opin. Genet. Dev. *67*, 94–102. https://doi.org/10.1016/j.gde.2020.12.001.
43. Los, G.V., Encell, L.P., McDougall, M.G., Hartzell, D.D., Karassina, N., Zimprich, C., Wood, M.G., Learish, R., Ohana, R.F., Urh, M., et al. (2008). HaloTag: A Novel Protein Labeling Technology for Cell Imaging and Protein Analysis. ACS Chem. Biol. *3*, 373–382. https://doi.org/10.1021/cb800025k.
44. Grimm, J.B., Xie, L., Casler, J.C., Patel, R., Tkachuk, A.N., Falco, N., Choi, H., Lippincott-Schwartz, J., Brown, T.A., Glick, B.S., et al. (2021). A General Method to Improve Fluorophores Using Deuterated Auxochromes. JACS Au *1*, 690–696. https://doi.org/10.1021/jacsau.1c00006.
45. Heckert, A., Dahal, L., Tjian, R., and Darzacq, X. (2022). Recovering mixtures of fast-diffusing states from short single-particle trajectories. eLife *11*, e70169. https://doi.org/10.7554/eLife.70169.
46. Chen, Y., Cattoglio, C., Dailey, G.M., Zhu, Q., Tjian, R., and Darzacq, X. (2022). Mechanisms governing target search and binding dynamics of hypoxia-inducible factors. eLife *11*, e75064. https://doi.org/10.7554/eLife.75064.
47. Hansen, A.S., Woringer, M., Grimm, J.B., Lavis, L.D., Tjian, R., and Darzacq, X. (2018). Robust model-based analysis of single-particle tracking experiments with Spot-On. eLife *7*, e33125. https://doi.org/10.7554/eLife.33125.
48. VanBelzen, J., Duan, C., Brickner, D.G., and Brickner, J.H. (2024). ChEC-seq2: an improved chromatin endogenous cleavage sequencing method and bioinformatic analysis pipeline for mapping in vivo protein–DNA interactions. NAR Genom. Bioinform. *6*, lqae012. https://doi.org/10.1093/nargab/lqae012.
49. Zentner, G.E., Kasinathan, S., Xin, B., Rohs, R., and Henikoff, S. (2015). ChEC-seq kinetics discriminates transcription factor binding sites by DNA sequence and shape in vivo. Nat. Commun. *6*, 8733. https://doi.org/10.1038/ncomms9733.
50. Heins, J.N., Suriano, J.R., Taniuchi, H., and Anfinsen, C.B. (1967). Characterization of a Nuclease Produced by Staphylococcus aureus.

J. Biol. Chem. *242*, 1016–1020. https://doi.org/10.1016/s0021-9258(18)96225-3.

51. Cunningham, L., Catlin, B.W., and de Garilhe, M.P. (1956). A Deoxyribonuclease of Micrococcus pyogenes. J. Am. Chem. Soc. *78*, 4642–4645. https://doi.org/10.1021/ja01599a031.
52. Schmid, M., Durussel, T., and Laemmli, U.K. (2004). ChIC and ChEC; genomic mapping of chromatin proteins. Mol. Cell *16*, 147–157.
53. Rossi, M.J., Kuntala, P.K., Lai, W.K.M., Yamada, N., Badjatia, N., Mittal, C., Kuzu, G., Bocklund, K., Farrell, N.P., Blanda, T.R., et al. (2021). A high-resolution protein architecture of the budding yeast genome. Nature *592*, 309–314. https://doi.org/10.1038/s41586-021-03314-8.
54. Zhang, Z., and Pugh, B.F. (2011). High-resolution genome-wide mapping of the primary structure of chromatin. Cell *144*, 175–186. https://doi.org/10.1016/j.cell.2011.01.003.
55. Rhee, H.S., and Pugh, B.F. (2011). Comprehensive genome-wide protein-DNA interactions detected at single-nucleotide resolution. Cell *147*, 1408–1419. https://doi.org/10.1016/j.cell.2011.11.013.
56. de Van de Vosse, D.W.V., Wan, Y., Lapetina, D.L., Chen, W.M., Chiang, J.H., Aitchison, J.D., and Wozniak, R.W. (2013). A role for the nucleoporin Nup170p in chromatin structure and gene silencing. Cell *152*, 969–983. https://doi.org/10.1016/j.cell.2013.01.049.
57. Li, Y., Lee, J., and Bai, L. (2024). DNA methylation-based high-resolution mapping of long-distance chromosomal interactions in nucleosome-depleted regions. Nat. Commun. *15*, 4358. https://doi.org/10.1038/s41467-024-48718-y.
58. Nishimura, K., Fukagawa, T., Takisawa, H., Kakimoto, T., and Kanemaki, M. (2009). An auxin-based degron system for the rapid depletion of proteins in nonplant cells. Nat. Methods *6*, 917–922. https://doi.org/10.1038/nmeth.1401.
59. Ariotti, N., Rae, J., Giles, N., Martel, N., Sierecki, E., Gambin, Y., Hall, T.E., and Parton, R.G. (2018). Ultrastructural localisation of protein interactions using conditionally stable nanobodies. PLoS Biol. *16*, e2005473. https://doi.org/10.1371/journal.pbio.2005473.
60. Yesbolatova, A., Saito, Y., Kitamoto, N., Makino-Itou, H., Ajima, R., Nakano, R., Nakaoka, H., Fukui, K., Gamo, K., Tominari, Y., et al. (2020). The auxin-inducible degron 2 technology provides sharp degradation control in yeast, mammalian cells, and mice. Nat. Commun. *11*, 5701. https://doi.org/10.1038/s41467-020-19532-z.
61. Rahmani, K., and Dean, D.A. (2017). Leptomycin B alters the subcellular distribution of CRM1 (Exportin 1). Biochem. Biophys. Res. Commun. *488*, 253–258. https://doi.org/10.1016/j.bbrc.2017.04.042.
62. Callanan, M., Kudo, N., Gout, S., Brocard, M.-P., Yoshida, M., Dimitrov, S., and Khochbin, S. (2000). Developmentally regulated activity of CRM1/XPO1 during early Xenopus embryogenesis. J. Cell Sci. *113*, 451–459. https://doi.org/10.1242/jcs.113.3.451.
63. Herzog, V.A., Reichholf, B., Neumann, T., Rescheneder, P., Bhat, P., Burkard, T.R., Wlotzka, W., von Haeseler, A., Zuber, J., and Ameres, S.L. (2017). Thiol-linked alkylation of RNA to assess expression dynamics. Nat. Methods *14*, 1198–1204. https://doi.org/10.1038/nmeth.4435.
64. Sun, M., Schwalb, B., Pirkl, N., Maier, K.C., Schenk, A., Failmezger, H., Tresch, A., and Cramer, P. (2013). Global Analysis of Eukaryotic mRNA Degradation Reveals Xrn1-Dependent Buffering of Transcript Levels. Mol. Cell *52*, 52–62. https://doi.org/10.1016/j.molcel.2013.09.010.
65. Sun, M., Schwalb, B., Schulz, D., Pirkl, N., Etzold, S., Larivière, L., Maier, K.C., Seizl, M., Tresch, A., and Cramer, P. (2012). Comparative dynamic transcriptome analysis (cDTA) reveals mutual feedback between mRNA synthesis and degradation. Genome Res. *22*, 1350–1359. https://doi.org/10.1101/gr.130161.111.
66. Baptista, T., Grünberg, S., Minoungou, N., Koster, M.J.E., Timmers, H.T.M., Hahn, S., Devys, D., and Tora, L. (2017). SAGA Is a General Cofactor for RNA Polymerase II Transcription. Mol. Cell *68*, 130–143.e5. https://doi.org/10.1016/j.molcel.2017.08.016.
67. Warfield, L., Ramachandran, S., Baptista, T., Devys, D., Tora, L., and Hahn, S. (2017). Transcription of Nearly All Yeast RNA Polymerase II-Transcribed Genes Is Dependent on Transcription Factor TFIID. Mol. Cell *68*, 118–129.e5. https://doi.org/10.1016/j.molcel.2017.08.014.
68. Haruki, H., Nishikawa, J., and Laemmli, U.K. (2008). The anchor-away technique: rapid, conditional establishment of yeast mutant phenotypes. Mol. Cell *31*, 925–932.
69. Neville, M., and Rosbash, M. (1999). The NES–Crm1p export pathway is not a major mRNA export route in Saccharomyces cerevisiae. EMBO J. *18*, 3746–3756. https://doi.org/10.1093/emboj/18.13.3746.
70. Larsson, A.J.M., Johnsson, P., Hagemann-Jensen, M., Hartmanis, L., Faridani, O.R., Reinius, B., Segerstolpe, Å., Rivera, C.M., Ren, B., and Sandberg, R. (2019). Genomic encoding of transcriptional burst kinetics. Nature *565*, 251–254. https://doi.org/10.1038/s41586-018-0836-1.
71. Costanzo, M., Baryshnikova, A., Bellay, J., Kim, Y., Spear, E.D., Sevier, C.S., Ding, H., Koh, J.L.Y., Toufighi, K., Mostafavi, S., et al. (2010). The genetic landscape of a cell. Science *327*, 425–431. https://doi.org/10.1126/science.1180823.
72. Cristea, I.M., Williams, R., Chait, B.T., and Rout, M.P. (2005). Fluorescent Proteins as Proteomic Probes. Mol. Cell. Proteomics *4*, 1933–1941. https://doi.org/10.1074/mcp.M500227-MCP200.
73. Kim, S.J., Fernandez-Martinez, J., Nudelman, I., Shi, Y., Zhang, W., Raveh, B., Herricks, T., Slaughter, B.D., Hogan, J.A., Upla, P., et al. (2018). Integrative Structure and Functional Anatomy of a Nuclear Pore Complex. Nature *555*, 475–482. https://doi.org/10.1038/nature26003.
74. Alber, F., Dokudovskaya, S., Veenhoff, L.M., Zhang, W., Kipper, J., Devos, D., Suprapto, A., Karni-Schmidt, O., Williams, R., Chait, B.T., et al. (2007). Determining the architectures of macromolecular assemblies. Nature *450*, 683–694. https://doi.org/10.1038/nature06404.
75. Alber, F., Dokudovskaya, S., Veenhoff, L.M., Zhang, W., Kipper, J., Devos, D., Suprapto, A., Karni-Schmidt, O., Williams, R., Chait, B.T., et al. (2007). The molecular architecture of the nuclear pore complex. Nature *450*, 695–701. https://doi.org/10.1038/nature06405.
76. Szoradi, T., Shu, T., Xie, Y., Kidiyoor, G.R., Herzog, N.L., Saxena, S., Bonucci, M., Brittingham, G., Lemiere, J., Keegan, S., et al. (2022). Genetically encoded multimeric (GEM) nanoparticles probe the biophysical properties of the nucleus. Biophys. J. *121*, 496a. https://doi.org/10.1016/j.bpj.2021.11.297.
77. Cibulka, J., Bisaccia, F., Radisavljević, K., Gudino Carrillo, R.M.G., and Köhler, A. (2022). Assembly principle of a membrane-anchored nuclear pore basket scaffold. Sci. Adv. *8*, eabl6863. https://doi.org/10.1126/sciadv.abl6863.
78. Dilworth, D.J., Suprapto, A., Padovan, J.C., Chait, B.T., Wozniak, R.W., Rout, M.P., and Aitchison, J.D. (2001). Nup2p dynamically associates with the distal regions of the yeast nuclear pore complex. J. Cell Biol. *153*, 1465–1478.
79. Denning, D., Mykytka, B., Allen, N.P., Huang, L., Al, B., and Rexach, M. (2001). The nucleoporin Nup60p functions as a Gsp1p-GTP-sensitive tether for Nup2p at the nuclear pore complex. J. Cell Biol. *154*, 937–950.
80. Folz, H., Niño, C.A., Taranum, S., Caesar, S., Latta, L., Waharte, F., Salamero, J., Schlenstedt, G., and Dargemont, C. (2019). SUMOylation of the nuclear pore complex basket is involved in sensing cellular stresses. J. Cell Sci. *132*, jcs224279. https://doi.org/10.1242/jcs.224279.
81. Komachi, K., and Burgess, S.M. (2022). The Nup2 meiotic-autonomous region relieves inhibition of Nup60 to promote progression of meiosis and sporulation in Saccharomyces cerevisiae. Genetics *221*, iyac045. https://doi.org/10.1093/genetics/iyac045.
82. Singh, D., Soni, N., Hutchings, J., Echeverria, I., Shaikh, F., Duquette, M., Suslov, S., Li, Z., van Eeuwen, T., Molloy, K., et al. (2024). The molecular architecture of the nuclear basket. Cell *187*, 5267–5281.e13. https://doi.org/10.1016/j.cell.2024.07.020.

83. Wen, W., Meinkoth, J.L., Tsien, R.Y., and Taylor, S.S. (1995). Identification of a signal for rapid export of proteins from the nucleus. Cell *82*, 463–473. https://doi.org/10.1016/0092-8674(95)90435-2.

84. Jumper, J., Evans, R., Pritzel, A., Green, T., Figurnov, M., Ronneberger, O., Tunyasuvunakool, K., Bates, R., Žídek, A., Potapenko, A., et al. (2021). Highly accurate protein structure prediction with AlphaFold. Nature *596*, 583–589. https://doi.org/10.1038/s41586-021-03819-2.

85. Port, S.A., Monecke, T., Dickmanns, A., Spillner, C., Hofele, R., Urlaub, H., Ficner, R., and Kehlenbach, R.H. (2015). Structural and Functional Characterization of CRM1-Nup214 Interactions Reveals Multiple FG-Binding Sites Involved in Nuclear Export. Cell Rep. *13*, 690–702. https://doi.org/10.1016/j.celrep.2015.09.042.

86. Koyama, M., Shirai, N., and Matsuura, Y. (2014). Structural Insights into How Yrb2p Accelerates the Assembly of the Xpo1p Nuclear Export Complex. Cell Rep. *9*, 983–995. https://doi.org/10.1016/j.celrep.2014.09.052.

87. Sumner, M.C., Torrisi, S.B., Brickner, D.G., and Brickner, J.H. (2021). Random sub-diffusion and capture of genes by the nuclear pore reduces dynamics and coordinates inter-chromosomal movement. eLife *10*, e66238. https://doi.org/10.7554/eLife.66238.

88. Sanborn, A.L., Yeh, B.T., Feigerle, J.T., Hao, C.V., Townshend, R.J., Lieberman Aiden, E.L., Dror, R.O., and Kornberg, R.D. (2021). Simple biochemical features underlie transcriptional activation domain diversity and dynamic, fuzzy binding to Mediator. eLife *10*, e68068. https://doi.org/10.7554/eLife.68068.

89. Pascual-Garcia, P., Jeong, J., and Capelson, M. (2014). Nucleoporin Nup98 associates with Trx/MLL and NSL histone-modifying complexes and regulates Hox gene expression. Cell Rep. *9*, 433–442. https://doi.org/10.1016/j.celrep.2014.09.002.

90. Franks, T.M., McCloskey, A., Shokirev, M.N., Benner, C., Rathore, A., and Hetzer, M.W. (2017). Nup98 recruits the Wdr82-Set1A/COMPASS complex to promoters to regulate H3K4 trimethylation in hematopoietic progenitor cells. Genes Dev. *31*, 2222–2234. https://doi.org/10.1101/gad.306753.117.

91. Bai, X.-T., Gu, B.-W., Yin, T., Niu, C., Xi, X.-D., Zhang, J., Chen, Z., and Chen, S.-J. (2006). Trans-Repressive Effect of NUP98-PMX1 on PMX1-Regulated c-FOS Gene through Recruitment of Histone Deacetylase 1 by FG Repeats. Cancer Res. *66*, 4584–4590. https://doi.org/10.1158/0008-5472.CAN-05-3101.

92. Kasper, L.H., Brindle, P.K., Schnabel, C.A., Pritchard, C.E.J., Cleary, M.L., and van Deursen, J.M.A. (1999). CREB Binding Protein Interacts with Nucleoporin-Specific FG Repeats That Activate Transcription and Mediate NUP98-HOXA9 Oncogenicity. Mol. Cell. Biol. *19*, 764–776. https://doi.org/10.1128/MCB.19.1.764.

93. Mendjan, S., Taipale, M., Kind, J., Holz, H., Gebhardt, P., Schelder, M., Vermeulen, M., Buscaino, A., Duncan, K., Mueller, J., et al. (2006). Nuclear pore components are involved in the transcriptional regulation of dosage compensation in Drosophila. Mol. Cell *21*, 811–823. https://doi.org/10.1016/j.molcel.2006.02.007.

94. Lu, H., Yu, D., Hansen, A.S., Ganguly, S., Liu, R., Heckert, A., Darzacq, X., and Zhou, Q. (2018). Phase-separation mechanism for C-terminal hyperphosphorylation of RNA polymerase II. Nature *558*, 318–323. https://doi.org/10.1038/s41586-018-0174-3.

95. Tyagi, S., Capitanio, J.S., Xu, J., Chen, F., Sharma, R., Huang, J., and Hetzer, M.W. (2023). High-precision mapping of nuclear pore-chromatin interactions reveals new principles of genome organization at the nuclear envelope. eLife *12*, RP87462. https://doi.org/10.1101/2021.05.10.443506.

96. Oka, M., Mura, S., Otani, M., Miyamoto, Y., Nogami, J., Maehara, K., Harada, A., Tachibana, T., Yoneda, Y., and Ohkawa, Y. (2019). Chromatin-bound CRM1 recruits SET-Nup214 and NPM1c onto HOX clusters causing aberrant HOX expression in leukemia cells. eLife *8*, e46667. https://doi.org/10.7554/eLife.46667.

97. Oka, M., Mura, S., Yamada, K., Sangel, P., Hirata, S., Maehara, K., Kawakami, K., Tachibana, T., Ohkawa, Y., Kimura, H., et al. (2016). Chromatin-prebound Crm1 recruits Nup98-HoxA9 fusion to induce aberrant expression of Hox cluster genes. eLife *5*, e09540.

98. Wang, X.Q.D., Fan, D., Han, Q., Liu, Y., Miao, H., Wang, X., Li, Q., Chen, D., Gore, H., Himadewi, P., et al. (2022). Mutant NPM1 hijacks transcriptional hub to maintain pathogenic gene programs in acute myeloid leukemia. Cancer Discov. *13*, 724–745. https://doi.org/10.1158/2159-8290.cd-22-0424.

99. Aumann, W.K., Heath, J.L., Conway, A.E., Sze, S.K., Gupta, V.K., Kazi, R.R., Tope, D.R., Wechsler, D.S., and Lavau, C.P. (2021). Fusion of the CRM1 nuclear export receptor to AF10 causes leukemia and transcriptional activation of HOXA genes. Leukemia *35*, 876–880. https://doi.org/10.1038/s41375-020-0998-3.

100. Hennig, B.P., Velten, L., Racke, I., Tu, C.S., Thoms, M., Rybin, V., Besir, H., Remans, K., and Steinmetz, L.M. (2018). Large-Scale Low-Cost NGS Library Preparation Using a Robust Tn5 Purification and Tagmentation Protocol. G3 (Bethesda) *8*, 79–89. https://doi.org/10.1534/g3.117.300257.

101. Longtine, M.S., McKenzie, A., 3rd, Demarini, D.J., Shah, N.G., Wach, A., Brachat, A., Philippsen, P., and Pringle, J.R. (1998). Additional modules for versatile and economical PCR-based gene deletion and modification in Saccharomyces cerevisiae. Yeast *14*, 953–961. https://doi.org/10.1002/(SICI)1097-0061(199807)14:10<953::AID-YEA293>3.0.CO;2-U.

102. Mazanka, E., Alexander, J., Yeh, B.J., Charoenpong, P., Lowery, D.M., Yaffe, M., and Weiss, E.L. (2008). The NDR/LATS Family Kinase Cbk1 Directly Controls Transcriptional Asymmetry. PLoS Biol. *6*, e203. https://doi.org/10.1371/journal.pbio.0060203.

103. Neumann, T., Herzog, V.A., Muhar, M., von Haeseler, A., Zuber, J., Ameres, S.L., and Rescheneder, P. (2019). Quantification of experimentally induced nucleotide conversions in high-throughput sequencing datasets. BMC Bioinform. *20*, 258. https://doi.org/10.1186/s12859-019-2849-7.

104. Love, M.I., Huber, W., and Anders, S. (2014). Moderated estimation of fold change and dispersion for RNA-seq data with DESeq2. Genome Biol. *15*, 550. https://doi.org/10.1186/s13059-014-0550-8.

105. Burke, D., Dawson, D., and Stearns, T. (2000). Methods in Yeast Genetics (CSHL Press).

106. Lõoke, M., Kristjuhan, K., and Kristjuhan, A. (2011). Extraction of genomic DNA from yeasts for PCR-based applications. Biotechniques *50*, 325–328. https://doi.org/10.2144/000113672.

107. Ariotti, N., Hall, T.E., Rae, J., Ferguson, C., McMahon, K.-A., Martel, N., Webb, R.E., Webb, R.I., Teasdale, R.D., and Parton, R.G. (2015). Modular Detection of GFP-Labeled Proteins for Rapid Screening by Electron Microscopy in Cells and Organisms. Dev. Cell *35*, 513–525. https://doi.org/10.1016/j.devcel.2015.10.016.

108. Udi, Y., Zhang, W., Stein, M.E., Ricardo-Lax, I., Pasolli, H.A., Chait, B.T., and Rout, M.P. (2023). A general method for quantitative fractionation of mammalian cells. J. Cell Biol. *222*, e202209062. https://doi.org/10.1083/jcb.202209062.

109. Bosch, B., DeJesus, M.A., Poulton, N.C., Zhang, W., Engelhart, C.A., Zaveri, A., Lavalette, S., Ruecker, N., Trujillo, C., Wallach, J.B., et al. (2021). Genome-wide gene expression tuning reveals diverse vulnerabilities of M. tuberculosis. Cell *184*, 4579–4592.e24. https://doi.org/10.1016/j.cell.2021.06.033.

110. Alalam, H., Zepeda-Martínez, J.A., and Sunnerhagen, P. (2022). Global SLAM-Seq for accurate mRNA decay determination and identification of NMD targets. RNA *28*, 905–915. https://doi.org/10.1261/rna.079077.121.

STAR★METHODS

KEY RESOURCES TABLE

REAGENT or RESOURCE	SOURCE	IDENTIFIER
Antibodies		
Goat Anti-Mouse IgG Antibody, Fc, HRP conjugate	Millipore-Sigma	Catalog#AP127P, RRID:AB_92472
Anti-Myc tag antibody [9E10]	Abcam	Catalog#ab32, RRID: AB_303599
Rabbit polyclonal anti-GFP	Abcam	Catalog#ab290, RRID: AB_2313768
Goat Anti-Rabbit IgG antibody (HRP)	Genetex	Catalog#GTX213110-01, RRID: AB_10618573
Anti-Myc tag antibody [9E10]	Abcam	Catalog#ab32, RRID: AB_303599
Rabbit polyclonal anti-GFP	Abcam	Catalog#ab290, RRID: AB_2313768
Bacterial and virus strains		
10-beta Competent *E. coli*	New England Biolabs	Catalog#C3019I
DH5α	Brickner lab stock	N/A
Chemicals, peptides, and recombinant proteins		
All chemicals unless otherwise noted	Sigma-Aldrich	N/A
Yeast media components	Sunrise Science Products	N/A
Restriction Enzymes	New England Biolabs	N/A
Indole-3-Acetic-Acid (3-IAA)	Gold Biotechnology	Catalog#1-110-100
5-phenyl-1H-indole-3-acetic acid (5-Ph-IAA)	Fisher Scientific	Catalog#NC1957890
Leptomycin B	Cayman Chemical Company	Catalog#10004976
Q5® High-Fidelity DNA Polymerase	New England Biolabs	Catalog#M0491L
Ex Taq® DNA Polymerase	TaKaRa	Catalog#RR001A
NEBuilder® HiFi DNA Assembly Master Mix	New England Biolabs	Catalog#E2621S
Stellaris RNA Hybridization Buffer	Biosearch Technologies, Inc.	Catalog#SMF-HB1-10
Stellaris RNA FISH Positive Control	Biosearch Technologies, Inc.	Catalog#T30-ATTO647N-1
Stellaris RNA FISH Wash Buffer A	Biosearch Technologies, Inc.	Catalog#SMF-WA1-60
Stellaris RNA FISH Wash Buffer B	Biosearch Technologies, Inc.	Catalog#SMF-WB1-20
Vectashield	Fisher Scientific	Catalog#NC9265087
Rapamycin	Sigma Chemicals	Catalog#553210-5MG
Formamide	Life Technologies	Catalog#AM9342
Formaldehyde	Fisher Scientific	Catalog#BP531-500
Janelia Fluor® JFX554 HaloTag® Ligand	Promega	Catalog#HT1030
Lysine-^{13}C6 ^{15}N2 lysine	Sigma-Aldrich	Catalog#608041-250MG
Dynabeads	Thermo Fisher Scientific	Catalog#14302D
NuPAGE™ Bis-Tris Protein Gels	Thermo Fisher Scientific	Catalog#NP0322
S-Traps	ProtiFi	S-Traps
HisTrapHP	Global Life Science Solutions	Catalog#17524802
C18 StageTips	Thermo Scientific	Catalog#87782
GSTraps	Global Life Science Solutions	Catalog#17528202
Digitonin	BioSynth International Inc	Catalog#XD175329
4-Thiouracil	Fisher Scientific	Catalog#AAH6191903
Estradiol	Sigma Aldrich	Catalog#E8875
Iodoacetamide	Sigma Aldrich	Catalog#I1149-5G
Lyticase	Sigma Aldrich	Catalog#L4025-1MU
Tn5 E54K L372P	Hennig et al.[100]	N/A
Roche cOmplete™, EDTA-free Protease Inhibitor Cocktail	Sigma Aldrich	Catalog#11873580001
Pierce™ Glutathione Magnetic Agarose	Thermo Scientific	Catalog#78601

(*Continued on next page*)

Continued

REAGENT or RESOURCE	SOURCE	IDENTIFIER
Critical commercial assays		
DNA Clean and Concentrate-5	Zymo	Catalog#NC9552153
Zymoclean Gel DNA Recovery Kit	Zymo	Catalog#D4001
QIAprep Spin Miniprep Kit	Qiagen	Catalog#27104
QuantSeq 3′ mRNA-Seq Library Prep Kit FWD	Lexogen	N/A
Pierce™ BCA Protein Assay Kits	Thermo Fisher Scientific	Catalog#23225
High Sensitivity RNA ScreenTape	Agilent Technologies Inc	Catalog#5067-5579
High Sensitivity RNA ScreenTape Sample Buffer	Agilent Technologies Inc	Catalog#5067-5580
Genomic DNA Screentape	Agilent Technologies Inc	Catalog#5067-5365
Genomic DNA Reagents	Agilent Technologies Inc	Catalog#5067-5366
High Sensitivity D5000 ScreenTape	Agilent Technologies Inc	Catalog#5067-5592
D5000 Reagents	Agilent Technologies Inc	Catalog#5067-5589
Alexa Fluor™ 488 Antibody Labeling Kit	Thermo Fisher Scientific	Catalog#Z11233
Deposited data		
Abf1 ChIP-exo	Rossi et al.[53]	SRP254928
Rap1 ChIP-exo	Rhee and Pugh[55]	SRR346373
Reb1 ChIP-exo	Rhee and Pugh[55]	SRR346400
Nup157 ChIP	Van de Vosse et al.[56]	GSM901171
Nup170 ChIP	Van de Vosse et al.[56]	GSM901172
Mlp1 MTAC	Li et al.[57]	From the authors
Experimental models: Organisms/strains		
Saccharomyces cerevisiae	See Strain Table	N/A
Oligonucleotides		
Table S8	IDT	N/A
Recombinant DNA		
pRSII402	Addgene	Catalog#35434
Plas-gRNA-LEU	Addgene	Catalog#309094
pAFS144	Straight et al.[34]	N/A
pFA6a-kanMX6	Longtine,et al.[101]	N/A
p5LacI-GFP	Egecioglu et al.[35]	N/A
pER04	Egecioglu et al.[35]	N/A
pZipKan	Egecioglu et al.[35]	N/A
p6LacO128	Brickner and Walter[12]	N/A
p6LacO128-LexABS	Randise-Hinchliff et al.[23]	N/A
p6LacO128-HIS4	Randise-Hinchliff et al.[23]	N/A
pELW749	Mazanka et al.[102]	N/A
p7-GFPrepI-LexA	Brickner et al.[29]	N/A
pMK419	Yesbolatova et al.[60]	N/A
pGEX-WT PD	this study	N/A
pET28a-PD-DBD-GST	this study	N/A
pGEX-TEV-PD-DBD	this study	N/A
pGEX-TEV-pdmt-DBD	this study	N/A
pET28a-GSP1	this study	N/A
pGEX4T-1-PKI NES	this study	N/A
pGEX6p-NUP2C	this study	N/A
pTG020	this study	N/A
pTG023	this study	N/A

(*Continued on next page*)

Continued

REAGENT or RESOURCE	SOURCE	IDENTIFIER
Software and algorithms		
R Studio	https://posit.co/downloads/	N/A
ZEN Imaging Software Version 3.6 Pro	ZEISS, Germany	N/A
saspt (package)	Heckert et al.[45]	N/A
Spot-On	Hansen et al.[47]	N/A
SpectroMine™	Biognosys AG	N/A
DoubleChEC	VanBelzen et al.[48]	N/A
SLAMDunk	Neumann et al.[103]	N/A
DESeq2	Love et al.[104]	N/A

EXPERIMENTAL MODEL AND STUDY PARTICIPANT DETAILS

All yeast strains were derived from the W303 *Saccharomyces cerevisiae* (RRID: NCBI:txid4932) strains CRY1 (*MAT***a** *ade2-1 ura3-1 trp1-1 his3-11,15 leu2-3,112 can1-100), CRY2 (MATα ade2-1 ura3-1 trp1-1 his3-11,15 leu2-3,112 can1-100*; Brickner and Fuller, 1997), or BY4741 (*MAT***a** *his3Δ1 leu2Δ0 lys2Δ0 ura3Δ0*) and are listed in Table S6. Cells were cultured in YPD (1% yeast extract, 2% peptone, 2% dextrose) or synthetic complete (SC) medium supplemented with the appropriate amino acids for inducing peripheral localization or expressing target genes at 30° C unless otherwise specified. *E. coli* (NCBI:txid469008) cultures were grown in LB + Ampicillin at 37° C. No human or animal participants were involved in this study.

METHOD DETAILS

Chemicals, media and growth conditions

Unless noted otherwise, chemicals were from Sigma-Aldrich (St. Louis, MO), restriction and modifying enzymes were from New England Biolabs (Ipswich, MA), DNA oligonucleotides were from Integrated DNA Technologies (Coralville, IA), yeast media components were from Sunrise Science Products (Knoxville, TN). Media were prepared as described[105] and yeast cultures were grown at 30° C in synthetic complete glucose (SDC) medium unless indicated otherwise. For peripheral localization experiments, cells were grown at room temperature (RT) in YPD overnight and then shifted to SDC (± histidine or ± inositol) for approximately 1h before imaging. For AID and grAID experiments, cells were grown overnight in SDC at RT, diluted in SDC and grown at 30° C for >4 h before being treated with either 500 μM Indole-3-Acetic Acid (3-IAA; AID Gold Biotechnology, catalog#I-110-100) for 1h or 1 μM estradiol (Sigma Aldrich, catalog# E8875) + 1 μM 5-Phenyl-1H-indole-3-acetic acid (5-Ph-IAA; Fisher Scientific, catalog# NC1957890), respectively, for 2h (grAID) prior to harvesting. Cultures for SLAM-seq were grown in SDC overnight, diluted in SDC and grown at 30° C for > 4h before switching into SDC-Ura + 2 mM 4-thiouracil (Fisher Scientific catalog # AAH6191903).

Yeast strains, plasmids, and molecular biology

All yeast strains were derived from the W303 strains CRY1 (*MAT***a** *ade2-1 ura3-1 trp1-1 his3-11,15 leu2-3,112 can1-100*), CRY2 (*MATα ade2-1 ura3-1 trp1-1 his3-11,15 leu2-3,112 can1-100*; Brickner and Fuller, 1997), or BY4741 (*MAT***a** *his3Δ1 leu2Δ0 lys2Δ0 ura3Δ0*) and are listed in Table S6. Yeast genomic DNA was extracted from strains using the protocol outlined in Looke et al., 2011.[106] DNA cleanup kits were from Zymo (catalog# D4014) and plasmid purification kits were from Qiagen (catalog # 27104). Oligonucleotides are listed in Table S8.

The *gcn4-pd* mutant strain (JBY536) was generated using CRISPR-Cas9 mediated mutagenesis of the Gcn4-GFP strain as described[29] using the following double stranded repair DNA: 5'- AGTCGTTAAGAAGTCACATCATGTTGGAAAGGATGACGAA TCcAGACTaGAcCAcCTAGGTGcTGccGCTgcCAACCGCAAACAGCGTTCGATTCCACTTTCTCCAATTGTG -3'. A wildtype strain (JBY537; *GCN4-sm*) with matching silent mutations in the guide sequence was generated using the following double stranded repair DNA: 5'-AGTCGTTAAGAAGTCACATCATGTTGGAAAGGATGACGAATCcAGACTaGAcCAcCTAGGTGTTGTTGCTTACAACCGCAA ACAGCGTTCGATTCCACTTTCTCCAATTGTG-3'. After evicting the CRISPR-Cas9 plasmid, mutant strains were confirmed by colony purifying, PCR amplification and DNA sequencing. To generate His$^-$ strains, the *His5MX* marker was replaced in JBY536 and JBY537 by transforming with the *KanMX* cassette and selecting for G418^r, His$^-$, generating JBY550 (*gcn4-pd*) and JBY551 (*GCN4-sm*). *LYS2* was then disrupted in these strains using *URA3* to produce Lys$^-$ His$^-$ GFP-tagged strains JBY557 (*gcn4-pd*) and JBY558 (*GCN4-sm*), which were used for SILAC mass spectrometry.

Leptomycin B (LMB)-sensitive reporter strain and parental strains with the T539C mutation were a gift from Dr. Eric Weiss (Northwestern University). This strain was transformed with LacO arrays, GFP-LacI, and pER04 membrane marker plasmids to generate strains for chromatin localization experiments.[35] GFP-tagged proteins in the LMB-sensitive strain were made via transformation and homologous recombination of PCR-amplified DNA with 50 bp of homology to the 3' end of the CDS of the proteins of interest. The GFP was amplified from a gBlock along with a Gly-Ser linker and *KanMX* marker. Successful transformations were confirmed by

PCR, sequencing around the insert, and imaging. LMB-sensitive strains were grown overnight in YPD before shifting into SDC ≥1h prior to imaging and treating with 185 nM LMB (Cayman Chemical Company, catalog# 10004976) at 30° C for 30 min prior to imaging.

MNase strains and the Crm1-Halo strain were constructed by amplifying the 3xFLAG-MNase with *KanMX* marker from pGZ108 with primers targeting the 3' end of the CDS of the protein of interest as previously described.[49] After transforming the PCR construct into cells and selecting with YPD+G418 plates, strains were confirmed by immunoblotting and sequencing. ChEC-seq2 was carried out as described.[48]

To generate Nup-LexA fusion proteins in strains from the GFP collection, LexA was swapped for GFP using a strategy similar to one described previously.[29] The p7-GFPrepI-LexA[29] insert was PCR amplified and transformed into 27 Nup-GFP strains. Transformants were plated on YPD+G418, screened for His^- and imaged by confocal microscopy for the loss of the GFP signal. Proper fusion and expression of selected NPC-LexA DBD proteins was confirmed by PCR and DNA sequencing as well as immunoblotting against LexA. The 27 *MAT***a** *Nup-LexA* fusion protein strains were crossed against *MATα* strains expressing LacI-GFP and the nuclear envelope/ER marker ER04[35] (mCherry) with either p6LacO128-LexABS or p6LacO128 integrated at *URA3*.[29] Diploid strains were selected on SDC-Ade,Ura plates. Similarly, we generated MNase-tagged fusions by replacing the GFP tag from strains in the GFP collection, FLAG-MNase or Halo was cloned in place of LexA from p7-GFPrepI-LexA, producing p7-GFPrepI-MNase and p7-GFPrepI-Halo. The GFP homology-MNase-ACT1 3'UTR – PRPL13A-KmR-ADH1 3'UTR - GFP homology was amplified by PCR and transformed into strains having Nup tagged with GFP. Fusions were confirmed by western blot and digestion of genomic DNA upon permeabilization with digitonin and addition of calcium.

Plasmids pAFS144,[34] pFA6a-kanMX6,[101] pER0410,[35] pZipKan,[35] p6LacO128,[12] p6LacO128-LexABS,[23] p6LacO128-HIS[24], pELW749, [102] and p7-GFPrepI-LexA[29] have been described. Plasmid p5LacI-GFP was derived from pAFS144: *HIS3* was removed from pAFS144 using *Aat*II and *Sac*I and replaced with *LEU2* from pRS305. Plasmid pRSII402-PADH-Gcn4$_{181-281}$ was made by cloning Gcn4 181-281 into pRSII402-PADH[23] as *Spe*I-*Xho*I fragment. Plasmid pGEX-WT PD was generated from pGEX4T-2 by cloning Gcn4 205-231 as a *Bam*HI fragment downstream of GST. The PD-DBD was cloned both upstream of GST into pET28a (pET28a-PD-DBD-GST; amino acids 189-281; Figure S6A) or downstream of GST in pGEX6p-2 (pGEX-TEV-PD-DBD and pGEX-TEV-pdmt-DBD; amino acids 181-281; Figures 7B, 7C, 7E, 7F, and S6D–S6G) because the GST-pdmt-DBD protein was better behaved than the pdmt-DBD-GST protein. The pET28a-GSP1 plasmid was made by cloning an *E. coli* codon-optimized gBLOCK (IDT) of the *GSP1* coding sequence as an *Nco*I + *Hin*dIII fragment into pET28a. The pGEX4T-1-PKI NES plasmid was constructed from oligonucleotides annealed and ligated into pGEX4T-1 digested with *Xho*I + *Bam*HI. Plasmid pGEX6p-NUP2C and pGEX6p-NUP2RBD were made by cloning an *E. coli* codon-optimized gBLOCK (IDT) encoding either amino acids 496-721 or 583-721 of Nup2, respectively. The pTG020 plasmid was constructed using PCR amplification of ostirF74G from pMK419 59, and of pRSII402 (Addgene, catalog#35434). Fragments were purified before mixing with HiFi Assembly Mastermix (NEB, catalog#E2621S) for 30 min at 50° C. Assemblies were transformed into 10-beta competent cells (NEB, catalog#C3019I) and plated onto LB agar plates for overnight incubation at 37°C. The next day, colonies were picked for overnight incubation in liquid LB at 37° C. After ~18 hours, colonies were purified and sent for whole plasmid sequencing through Primordium Labs. For grAID, plasmid pTG020 digested with *Stu*I was transformed into yeast. Plasmid pTG023 was constructed using PCR amplification of Plas-gRNA-LEU (Addgene, #309094), a gBLOCK (IDT) designed to fuse csGBP[107] and mAID.[60] Fragments were assembled and confirmed via sequencing and pTG023 digested with *Eco*RV was transformed into yeast.

Microscopy

Chromatin localization

Chromatin localization experiments were carried out as described[35] on a Leica SP-8 confocal microscope (Northwestern Biological Imaging Facility). Briefly, z-stacks of ≥ 5μm, comprising the whole yeast cell, were collected and gene positioning was scored within the slice with the most focused, intense LacO/LacI-GFP spot. For experiments in which we scored peripheral localization, ≥ 30 cells were scored per biological replicate and at least three biological replicates were scored for each strain or condition.

RNA FISH

Subcellular localization of poly A+ RNA was assessed using Stellaris RNA FISH products from LGC, Biosearch Technologies (Petaluma, CA.) All samples were prepared as described in Stellaris RNA FISH protocol for *Saccharomyces cerevisiae*. Approximately 10 ODs of log-phase yeast cells were fixed with 3.7% formaldehyde for 45 min at room temperature. Cells were harvested at 1600 x g for 5 min and resuspended in 1 ml ice-cold Fixation buffer (1.2 M Sorbitol, 0.1 M Potassium phosphate dibasic, pH7.5) and spheroplasted with 2.5 μl lyticase for ~90 min at 37° C, spun at 400 x g for 5 min before permeabilizing in 70% ethanol overnight at 4° C. Following permeabilization, cells were resuspended in 100 μl of Stellaris RNA FISH Hybridization Buffer (catalog# SMF-HB1-10) containing 10% formamide and 125 nM poly T probe (catalog# T30-ATTO647N-1) and incubated at 30° C overnight in the dark. After hybridization, 100μl of Stellaris RNA FISH Wash Buffer A (catalog# SMF-WA1-60) containing 10% formamide was added before centrifugation at 400 x g for 5 min. Hybridized cells were washed in 1 ml Wash Buffer A at 30° C in the dark for 30 minutes. Cells were collected at 400 x g for 5 min, resuspended in 1 ml Wash Buffer A, with 5 ng DAPI to counterstain nuclei at 30° C in the dark for 30 min. Cells were pelleted at 400 x g for 5 min then resuspended in Wash Buffer B (catalog# SMF-WB1-20) at 30C for 5 min. Cells were then pelleted at 400 x g for 5 min and resuspended in 25μl Vectashield (Fisher Scientific, catalog# NC9265087). A small volume of the Vectashield-suspended cells was placed on a poly-lysine-treated slide and imaged on a Leica SP8 confocal microscope in the Northwestern University Biological Imaging Facility.

Live-cell, single-molecule tracking

Sample preparation

Crm1-Halo was made by homologous recombination to introduce the Halo tag and *KanMX* marker, as described above. The *PDR5* gene was subsequently deleted using the *LEU2* marker. Crm1-Halo was labeled with 40 nM JFX554 (Promega, catalog# HT1030) at 30°C in Complete Supplement Mixture (CSM) supplemented with 80 mg/L adenine hemisulfate. After 4 hours of labeling, mid-log culture (OD600 ~0.8) was harvested and washed with ~1 mL CSM+Ade five times to remove excess JFX554.

A coverslip (#1.5, ø 25 mm, Electron Microscopy Services) was heat-treated, coated with Concanavalin A (0.5 mg/mL), and assembled in a metal Attofluor chamber (ø 35 mm, Invitrogen). Washed cells (1 mL) were added and allowed to attach to the coverslip for 2 min, followed by gentle rinses with fresh CSM to achieve a monolayer. Cells were imaged in 1 mL of CSM. Because each imaging session lasted ~90 min, we replaced CSM every 30 min min to avoid local nutrient depletion for immobilized cells.

Single-molecule imaging

Imaging was carried out at room temperature on an Axio Observer 7 microscope (Zeiss, Germany) equipped with an α-Plan-Apochromat 150x/1.35 glycerin-immersion objective (ZEISS, Germany). JFX554 was excited with a 552 nm laser (OBIS LS, Coherent) and a filter cube containing a quadband dichroic (ZT405/488/555/640rpc-UF2, 25.5 x 36 x UF2mm, Chroma) and emission filter (ET595/44m, Chroma). Images were acquired with an EM-CCD camera (C9100-23B, Hamamatsu Photonics, Japan) featuring 512x512 16 μm pixels and operating at -80° C (forced-air cooling) and 500x EM gain. The pixel size of recorded images is 107 nm. The ZEN imaging software (Version 3.6 Pro, ZEISS, Germany) operated the microscope and camera. For fast tracking, we excited the sample with ~1 kW/cm^2 continuous laser and imaged a 208x208 pixel field of view (containing ~8 single cells) for 1 min at 10 ms (100Hz) frame rate. Single Crm1-Halo molecules were tracked with ~37 nm accuracy (Table S2) at 100 Hz using STORM illumination.

Single-molecule data processing and analysis

We localized and tracked single Crm1-Halo molecules as previously described.[41] Most Crm1 localized to the nucleus (Figures 1G and S1B) and extranuclear Crm1 was computationally excluded. SMT produced consistent results across three biological replicates (Table S2), comprising over 15,000 individual tracks. We then used the saspt package[45] for track-based modelling of Crm1 diffusivities. To quantify distinct bound, slow, and free behaviors, we performed displacement-based three-state kinetic modeling using the Spot-On[47] web interface (https://spoton.berkeley.edu/). Fitting parameters and results are summarized in Table S2.

Stable Isotope Labelling by Amino acids in Cell culture (SILAC) mass spectrometry

WT Gcn4 strain JBY558 was cultured media with 0.1 mg/ml Lysine-^{12}C6 ^{14}N2 lysine and the *gcn4-pd* mutant strain JBY557 was cultured in media with 0.1 mg/ml lysine-^{13}C6 ^{15}N2 lysine overnight and then shifted for 1 hour into 2L SDC-His + heavy or light lysine before harvesting. Cells were harvested by filtration, scraped into a syringe and frozen as noodles. Cells were cryo-milled in a Retch MM400 3 x 3min at 30Hz. 5g yeast lysate powder was resuspended on 40ml cold lysis buffer (20mM HEPES-KOH pH 7.4, 50mM KOAc, 20mM NaCl, 0.5% Triton-X100, 0.1% Tween-20, 2 mM MgCl2, 10% glycerol, 1mM DTT + protease inhibitors (1 mM PMSF; 1 μg/ml Leupeptin; 1 μg/ml Pepstatin A; 10 μg/ml Aprotinin)) by vortexing. Insoluble material was removed by centrifugation at 10,000 x g, 10 min and 2mM glutaraldehyde was added to the lysate. After 5 min, glutaraldehyde was quenched with 50 mM of lysine. The lysate was added to 50μl sepharose coupled with LaG16 anti-GFP nanobody. Beads were rotated for 1 hour at 4° C, washed three times in lysis buffer. Affinity purified proteins were eluted with SDS sample buffer and pooled, separated on replicate lanes on a 10% SDS PAGE gels. After staining, each lane was cut into 20 equal size slices, each of which was subjected to quantitative tandem mass spectrometry at the Northwestern University Proteomics Facility.

Purification of Crm1-x-GFP and Nup2-x-GFP

Anti-GFP pulldown experiments were performed as described,[37] with the following modifications. After cryomilling, 1g of Crm1-x-GFP or 2g of Nup2-x-GFP powder was resuspended in 8 ml of either Crm1 pulldown buffer (20mM HEPES-KOH pH7.4 250mM Na Citrate 150mM KOAc 0.1% Triton X-100 + protease inhibitors (see above)) or Nup2 pulldown buffer (20mM HEPES pH7.4 0.5% Triton X-100 0.1% Tween-20 250mM Sodium Citrate 150mM NaCl), respectively. The powder mixture was vortexed to resuspend and the lysate was spun 10 min at 11,000 rpm in Beckman JLA 16.250 rotor. The supernatant was added to 5mg M-270 Epoxy Dynabeads (ThermoFisher, catalog# 14301) coupled with LaG94-10 nanobody and incubated 30 min at 4° C as described.[37] The beads were harvested on a magnetic rack, washed three times in the respective pulldown buffer and resuspended in 20μl 5% SDS 500mM NH4OH and heated at 70° C, 5 min. The beads were removed on a magnetic rack and the supernatant was collected. 5μl of the eluate was run on a 4-12% NuPAGE gel (Invitrogen, catalog# NP0321BOX) and the remainder was dried in a Speedvac for 2 hours, with heating.

Samples were processed for mass spectrometry as described[108,109] with the following modifications: peptides were generated from proteins using S-Traps (ProtiFi, Fairport NY) according to the manufacturer. Peptides were then purified over a C18 StageTips (Pierce) and analyzed by LC-MS using an Orbitrap Exploris mass spectrometer coupled with an Easy-nLC system (Thermo Fisher Scientific). SpectroMine software (Biognosys AG) was used for label-free quantitation (LFQ). To compare LFQs across biological replicates, proteins were normalized to the antigen.

ChEC seq2 and SLAM-seq and data analysis

ChEC-seq2 and data analysis in R were performed as described.[48] For the grAID experiment (Figure 3), cleavage was carried out in SDC + digitonin (BioSynth, catalog# XD175329) + 2mM calcium. SLAM-seq was performed as described.[63,110] Yeast cells were grown in synthetic complete medium containing glucose (SDC) before Crm1 was inhibited by treating the cultures with 185 nM leptomycin B (LMB) in ethanol for 30 min at 30° C. Nup2 was degraded by treating *NUP2-AID* cells with 500 μM indole-3-acetic acid (3-IAA) in ethanol for 16 hours at 30° C. Prior to harvesting, cultures were treated with 0.2 mM 4- thiouracil (4sU; Fisher Scientific, catalog#AAH6191903), for 6 min at 30° C and then cells were spun down and snap frozen. Total RNA was extracted using Phenol:Chloroform:IAA (25:24:1), precipitated and 5 ug total RNA was treated with 10 mM iodoacetamide (Sigma-Aldrich, catalog# I1149), for 15 min at 50° C. Sequencing libraries were made using the QuantSeq 3'mRNA-seq Library Prep Kit for Illumina (FWD; Lexogen) following manufacturer's protocol. All experiments had at least three biological replicates. SLAM-seq data was analyzed by SLAM-DUNK[63] and DESeq2[104] was used to identify mRNAs and nascent transcripts that changed significantly.

Nup2-Mediator genetic interactions

Nup2-AID + mediator knockout strains were created by transforming the *NUP2-AID* strain with PCR products having *HIS3* from plasmid pFA6a-His3MX6 and 45bp arms matching sequences upstream and downstream of the coding sequence of each Mediator gene (see Oligos). After confirming the knockout via PCR, strains were treated with 500 μM 3-IAA in ethanol or solvent for 1 hour at 30° C and then diluted to 0.1 OD. 300 μl of diluted cells was placed in each well in triplicate in a 96-well plate. OD_{600} was measured at 30°C with every 20 min for 24 hr-40 hours using a 96-well plate reader (BioTek Synergy) without shaking. At least three biological replicates were performed for each strain and mutant.

Doubling time (T_d) is the time for a population to double in size. During exponential growth, population size at any time, n(t), can be calculated from the initial population size (n_0), the time elapsed (t) and the growth rate (r) as follows:

$$n(t) = n_0 * e^{rt}$$

Because the doubling time (T_d) results in

$$n(t) = 2 * n_0$$

We can simplify the equation for n to:

$$2 = e^{rT_d}$$

Which can be rearranged to solve for T_d:

$$T_d = ln(2)/r$$

Because r is equal to the slope of the growth curve, we calculated T_d using this formula from the tangent at every time 20-min point. From minimal doubling time (T_{dmin}), we calculated the maximum growth rate ($GR = ln(2)/T_{dmin}$) and the earliest time point at which this rate was observed we define as the lag time (as illustrated in Figure 5D and listed in Table S4). Thus, high fitness is associated with a larger growth rate and a shorter lag. Inactivation of either Nup2 or Mediator subunits reduced growth rate and increased lag compared with the wild type strain (*i.e.*, *NUP2-AID* – IAA in Table S4). The fitness effects of a mutation can be expressed as either the maximal growth rate of the mutant divided by the maximal growth rate of the wild type or the lag time of the mutant divided by the lag time of the wild type. A fitness defect corresponds to a growth rate ratio < 1 and a lag phase ratio > 1. Because the strains were all *NUP2-AID*, the *NUP2-AID* -IAA served as the wild type. The expected fitness effects of Nup2 depletion (Figure 5D) were calculated as:

$$NUP2AID\ GR\ phenotype = \frac{GR\ of\ Nup2AID\ WT + \mathrm{IAA}}{GR\ of\ Nup2AID\ WT\ -\ IAA}$$

and

$$NUP2AID\ lag\ phenotype = \frac{lag\ of\ Nup2AID\ WT + \mathrm{IAA}}{lag\ of\ Nup2AID\ WT\ -\ IAA}$$

The fitness effects for each Mediator subunit was calculated as:

$$med\Delta GR\ phenotype = \frac{GR\ of\ med\Delta Nup2AID\ -\ \mathrm{IAA}}{GR\ of\ Nup2AID\ WT\ -\ IAA}$$

and

$$med\Delta lag\ phenotype = \frac{lag\ of\ med\Delta Nup2AID\ -\ \mathrm{IAA}}{lag\ of\ Nup2AID\ WT\ -\ IAA}$$

Finally, the fitness effects of each double mutant was calculated as:

$$medΔNUP2AID\ GR\ phenotype = \frac{GR\ of\ medΔNup2AID + IAA}{GR\ of\ Nup2AID\ WT\ -\ IAA}$$

and

$$medΔNUP2AID\ lag\ phenotype = \frac{lag\ of\ medΔNup2AID + IAA}{lag\ of\ Nup2AID\ WT\ -\ IAA}$$

To calculate the expected effects of additive phenotypes for the *medΔ NUP2-AID* upon addition of auxin, the fitness ratios of each single mutant were multiplied (Table S4, columns J & K). In other words, if Nup2 depletion led to a growth rate ratio of 0.8 and a lag ratio of 1.2 and *medΔ* led to a growth rate ratio of 0.7 and a lag ratio of 1.5, then the expected values for *medΔ* Nup2-AID + auxin would be a growth rate ratio 0.8 x 0.7 = 0.56 and a lag ratio of 1.2 x 1.5 =1.8. We then calculated the ratio of the observed growth rates and lags to the expected growth rates and lags (Table S4, columns L & M). Additive phenotypes should match the expected values, giving a value of 1 for growth rate and lag (meaning that the expected equals the observed; $\log_2$ ratio = 0; white dot in Figure 5E). More-than-additive synthetic sick interactions would lead to an observed growth rate that is less than expected (negative $\log_2$ ratio) and an observed lag that is larger than expected (positive $\log_2$ ratio; blue quadrant in Figure 5D). Finally, less-than-additive buffering genetic interactions would lead to an observed growth rate that is greater than expected (positive $\log_2$ ratio) and an observed lag that is less than expected (negative $\log_2$ ratio; red quadrant in Figure 5E).

grAID (green fluorescent protein-targeted AID)

grAID strains were grown in SDC overnight at RT or 30° C before diluting in SDC the next day and growing at 30° C for > 4 hours. Cells were then treated with 1 μM estradiol (E2; Sigma Aldrich, catalog# E8875) for 30 min at 30° C before treating with 1 μM of 5-Ph-IAA (Fisher Scientific, catalog# NC1957890) for 2 hours at 30° C and harvesting for immunoblotting and ChEC-seq2.

Protein purification and labeling

H_6-Crm1 was expressed in BL21(DE3) and purified as described.[102] GST-Crm1, GST-Crm1 T539C, H_6-GSP1, GST-NES, GST-NUP2C, GST, GST-DBD, GST-PD, and GST-PD-DBD in BL21(DE3) were grown on an LB agar plate with ampicillin or kanamycin at 37° C overnight following plasmid transformation. Cells were resuspended into 2L LB + antibiotic medium and grown to OD_{600} = 0.6-0.7. IPTG was added to 0.5mM and cells were shifted to 18° C overnight, harvested, washed in water and then resuspended in 50ml lysis buffer (GST proteins: 20mM HEPES pH7.4, 400mM NaCl, 1mM EDTA 2mM DTT and protease inhibitors (see above); His-tagged proteins: 20mM HEPES pH7.4, 400mM NaCl, 1mM DTT and protease inhibitors) and frozen in 2 x 25ml tubes in liquid N_2. Cells were thawed and lysed in an Avestin C3 high pressure homogenizer (4 x 15,000 psi). For GST-DBD and GST-PD-DBD lysates, nucleic acids were precipitated by addition of 1ml 5% polyethylene amine while mixing. Insoluble material was removed by centrifugation 30-60 min at 40,000 rpm in a Beckman TLS55. To the supernatant, NaCl was added to 1M and passed over a 5ml GSTrap column using a peristaltic pump. The column was washed 1 x 10ml lysis buffer + 1M NaCl and then transferred to an AKTA Purifier FPLC, where it was washed with 20ml lysis buffer and then eluted over a 0-100% gradient of (GST proteins: 20mM HEPES pH 7.4, 150mM KOAc, 40mM glutathione, 1mM EDTA, 2mM DTT; His-tagged proteins: 20mM HEPES pH 7.4, 150mM KOAc, 250mM imidazole, 1mM DTT). Fractions were analyzed by SDS PAGE, and peak fractions were pooled and dialyzed overnight into storage buffer (20mM HEPES pH 7.4 150mM KOAc, 1mM EDTA, 2mM DTT).

For experiments in which tags were removed from Crm1 or Nup2C, the peak fractions were incubated with PreScission protease for > 2 hours on ice. Crm1 was purified away from the protease and the GST tag by gel filtration (S-200 Superdex). GST and the protease were depleted after cleavage of GST-Nup2C by passing over GSTrap and HisTrap columns. Ammonium sulfate was added to Nup2C to 1M and the protein was bound to Phenyl sepharose, washed with 20mM HEPES pH 7.4 150mM KOAc, 1mM EDTA, 1mM DTT, 1M ammonium sulfate and then eluted with 0-100% 20mM HEPES pH 7.4 150mM KOAc, 1mM EDTA, 1mM DTT. After cleavage of GST-Gcn4 PD-DBD, the PD-DBD (aa 181-281) was bound to a 5 ml HiTrap S column, washed with 10ml 20mM HEPES pH 7.4 150mM KOAc, 1mM EDTA, 2mM DTT, and eluted with a gradient of 0-100% 10ml 20mM HEPES pH 7.4 2.5M NaCl, 1mM EDTA, 2mM DTT, pooled peak fractions, and dialyzed into 20mM HEPES pH 7.4 150mM KOAc, 1mM EDTA, 2mM DTT overnight at 4° C. Purified proteins were aliquoted, frozen in N_2, and stored at -80° C. Aliquots were only thawed once. Ran was loaded with nucleotide by combining 100-200μM H_6-Gsp1 with 10mM Mg-GDP or Mg-GTP and incubating at 37° C for 20 min.

For Gcn4 fluorescence polarization experiment, 110μl of 40μM Gcn4 PD-DBD was labeled using the AlexaFluor 488 labeling kit (Thermo Fisher Scientific, catalog# Z11233) according to the manufacturer's instructions. The reaction was quenched by addition of 900μl 100mM Tris pH7.5 and purified using a 3000 MWCO concentrator spin filter.

GST pulldown experiments

For each lane, 5 μl glutathione magnetic beads were used. Beads were equilibrated in pulldown buffer (20mM HEPES pH 7.4, 150mM KOAc, 10% PEG_{2050}, 1mM EDTA 2mM DTT) and then loaded with 1.5 nmoles of GST fusion protein for 20 min at room temperature. Unbound protein was removed by washing three times with pulldown buffer. Beads were resuspended in the binding reaction with

the indicated concentrations of proteins, incubated with rotation at room temperature for 20 min. Beads were recovered on the magnet, washed 3 x 100μl pulldown buffer and proteins were eluted in 30μl 20mM HEPES pH7.4, 40mM glutathione. The eluate was added to 5μl 1% sodium deoxycholate, mixed, and precipitated in 10% trichloroacetic acid (TCA). The TCA pellet was washed with cold acetone, dried, suspended in 25μl sample buffer and heated at 65° C, 5 min. 10μl of the sample was loaded onto 10% polyacrylamide gels and run in MES buffer 100V 1.5 hours and stained with Coomassie blue.

Electrophoretic Mobility Shift Assay

In 20μl reactions containing 20% glycerol, 100mM KCl, 20mM HEPES pH 6.8, 0.2mM EDTA, and 0.042% bromophenol blue, DNA binding proteins, and other factors were combined with 5pmoles AlexaFluor488-labeled Gcn4 binding site + 50μg poly dIdC ± 1μM Crm1 ± 1μM Ran-GTP or 1μM Nup2C. Reactions were incubated for 15 minutes at room temperature and then separated on a 6% DNA retardation gel in 0.5X TBE running buffer (ThermoFisher). The gel was imaged with a SapphireTM multimode imager in the Keck Biophysics facility at Northwestern University.

QUANTIFICATION AND STATISTICAL ANALYSIS

All statistical analysis was performed using R version 4.3.1. When averages were reported, they were calculated from three or more biological replicates (i.e. $n \geq 3$) and error bars represent the standard error of the mean (SEM). For localization experiments (Figures 1, 3, 6, 7, and S5), $\geq$ 30 cells were scored per biological replicate, Student's t-test was used to compare peripheral localization and asterisks indicate $p < 0.05$. For Figure 2, we performed a Fisher's exact test to see if genes from ChEC-seq2 of Crm1 and Nups (Nup1, Nup2, Nup60) and ChIP-exo of transcription factors overlap more than expected by chance. We then took the Bonferroni-adjusted p-value and plotted it against the total number of overlapping genes (Figure 2E). For MEME (Figure 2F), an E-value was calculated for each motif, which represents the number of motifs that would have equal or higher log likelihood ratio if the input sequence order was shuffled or generated randomly, highlighting the statistical significance of the motif. In Figure 5A, the cor function in R was used to calculate the Spearman correlation coefficient between $\log_2$ of Crm1/Nup cleavage vs $\log_2$ of Rpb1-MNase cleavage over -700 bp to -125 bp from transcriptional start site for all yeast genes. For Figure 6E, the heatmaps represent either the label-free quantification (LFQ) from indicated proteins (co-precipitating with either Crm1 or Nup2) normalized to the stoichiometries of the proteins in the NPC or the peripheral localization (% of cells) found in strains with Nup-LexA fusions and a LexA Binding Site at ectopic locus *URA3*.